

# Assessing the accuracy of 1-D analytical heat tracing for estimating near-surface sediment thermal diffusivity and water flux under transient conditions

Rau, Gabriel C.; Cuthbert, Mark O.; McCallum, Andrew M.; Halloran, Landon J S; Andersen, Martin S.

DOI:  
[10.1002/2015JF003466](https://doi.org/10.1002/2015JF003466)

*Document Version*  
Peer reviewed version

*Citation for published version (Harvard):*

Rau, GC, Cuthbert, MO, McCallum, AM, Halloran, LJS & Andersen, MS 2015, 'Assessing the accuracy of 1-D analytical heat tracing for estimating near-surface sediment thermal diffusivity and water flux under transient conditions', *Journal of Geophysical Research: Earth Surface*, vol. 120, no. 8, pp. 1551-1573.  
<https://doi.org/10.1002/2015JF003466>

[Link to publication on Research at Birmingham portal](#)

## General rights

Unless a licence is specified above, all rights (including copyright and moral rights) in this document are retained by the authors and/or the copyright holders. The express permission of the copyright holder must be obtained for any use of this material other than for purposes permitted by law.

- Users may freely distribute the URL that is used to identify this publication.
- Users may download and/or print one copy of the publication from the University of Birmingham research portal for the purpose of private study or non-commercial research.
- User may use extracts from the document in line with the concept of 'fair dealing' under the Copyright, Designs and Patents Act 1988 (?)
- Users may not further distribute the material nor use it for the purposes of commercial gain.

Where a licence is displayed above, please note the terms and conditions of the licence govern your use of this document.

When citing, please reference the published version.

## Take down policy

While the University of Birmingham exercises care and attention in making items available there are rare occasions when an item has been uploaded in error or has been deemed to be commercially or otherwise sensitive.

If you believe that this is the case for this document, please contact [UBIRA@lists.bham.ac.uk](mailto:UBIRA@lists.bham.ac.uk) providing details and we will remove access to the work immediately and investigate.

1 **Assessing the accuracy of 1-D analytical heat tracing for estimating near-surface sediment**  
2 **thermal diffusivity and water flux under transient conditions**

3 Revised manuscript for resubmission to the [\*Journal of Geophysical Research \(Earth Surface\)\*](#)

4 Gabriel C. Rau<sup>\*1</sup>, Mark O. Cuthbert<sup>1, 2</sup>, Andrew M. McCallum<sup>3</sup>, Landon J.S. Halloran<sup>1</sup>, Martin  
5 S. Andersen<sup>1</sup>

6

7 1. Connected Waters Initiative Research Centre, School of Civil and Environmental  
8 Engineering, Water Research Laboratory, UNSW Australia, Manly Vale 2093 NSW,  
9 Sydney, Australia

10 2. School of Geography, Earth and Environmental Sciences, University of Birmingham,  
11 Edgbaston, Birmingham, B15 2TT, UK

12 3. Affiliated with the Connected Waters Initiative Research Centre, UNSW Australia, Manly  
13 Vale, Australia

14

15 \* Corresponding Author:

16 Gabriel C. Rau ([gabriel.rau@unsw.edu.au](mailto:gabriel.rau@unsw.edu.au))

17 UNSW Australia, Water Research Laboratory, 110 King Street, Manly Vale 2093, Australia

18 Phone: +61 2 8071 9850, Fax: +61 2 9949 4188

19

20 Keywords: Heat as a tracer, scour/depositional processes, transient water flux, temperature  
21 records, harmonic signal extraction.

22 **Abstract**

23 Amplitude decay and phase delay of oscillating temperature records measured at two vertical  
24 locations in near-surface sediments can be used to infer transient water fluxes, thermal  
25 diffusivity and sediment scour/deposition. While methods that rely on the harmonics-based  
26 analytical heat transport solution assume a steady-state water flux, many applications have  
27 reported transient fluxes, but ignored the possible violation of this assumption in the method.  
28 Here, we use natural heat tracing as an example to investigate the extent to which changes in the  
29 water flux, and associated temperature signal non-stationarity, can be separated from other  
30 influences. We systematically scrutinize the assumption of steady-state flow in analytical heat  
31 tracing and test the capabilities of the method to detect the timing and magnitude of flux  
32 transients. A numerical model was used to synthesize the temperature response to different step  
33 and ramp changes in advective thermal velocity magnitude and direction for both a single-  
34 frequency and multi-frequency temperature boundary. Time-variable temperature amplitude and  
35 phase information were extracted from the model output with different signal processing  
36 methods. We show that a worst-case transient flux induces a temperature non-stationarity, the  
37 duration of which is less than 1 cycle for realistic sediment thermal diffusivities between 0.02-  
38 0.13 m<sup>2</sup>/d. However, common signal processing methods introduce erroneous temporal  
39 spreading of advective thermal velocities and significant anomalies in thermal diffusivities or  
40 sensor spacing, which is used as an analogue for streambed scour/deposition. The most time-  
41 variant spectral filter can introduce errors of up to 57 % in velocity and 33 % in thermal  
42 diffusivity values with artifacts spanning  $\pm 2$  days around the occurrence of rapid changes in flux.  
43 Further, our results show that analytical heat tracing is unable to accurately resolve highly time-  
44 variant fluxes and thermal diffusivities and does not allow for the inference of scour/depositional  
45 processes due to the limitations of signal processing in disentangling flux-related signal non-  
46 stationarities from those stemming from other sources. To prevent erroneous interpretations,  
47 hydrometric data should always be acquired in combination with temperature records.

## 48 **1. Introduction**

49 Many measured signals that fluctuate over time exhibit amplitude decay and phase shifting over  
50 space caused by time-varying natural processes, for example: seismic wave propagation [Best et  
51 al., 1994], depth profiles of soil moisture [Wu et al., 2002], groundwater levels [Cuthbert, 2010]  
52 and seafloor temperature depth profiles [Goto et al., 2005]. In water-saturated near-surface  
53 aquatic systems natural heat has become a popular tracer to quantify vertical water fluxes  
54 [Anderson, 2005; Rau et al., 2014]. This is due to the presence of daily temperature fluctuations  
55 on the earth's surface [Stallman, 1965], increasing interest in surface-groundwater exchange  
56 fluxes, and developments in measurement technology to miniaturize and automate sensors  
57 [Constantz, 2008]. In particular, analytical approaches to invert water fluxes from multi-level  
58 temperature records have received much attention and are now common practice. Constantz  
59 [2008] correctly predicted that heat tracing will elevate the significance of streambed research to  
60 a field of "streambed science".

61 Few publications in this field of research have sparked as much follow-on research as Suzuki's  
62 [1960] and Stallman's [1965] original presentation of the analytical solution to the 1D  
63 convective-conductive heat transport equation with a sinusoidal temperature boundary at the top  
64 and a constant temperature boundary at infinite depth. Stallman's [1965] model is an extension  
65 to the harmonically-forced solution developed by Carslaw and Jaeger [1959], allowing for  
66 movement of water by including the first order spatial derivative of temperature. As such, it  
67 could be a mathematical description for many physical processes that are gradient driven and  
68 adhere to a simplified homogeneous linear second order differential equation.

69 Stallman's [1965] analytical solution has inspired various method developments and  
70 applications. Goto et al. [2005] successfully estimated sediment thermal regimes and the steady-  
71 state vertical water flux near a hydrothermal mound at the ocean floor. Hatch et al. [2006]  
72 dissected the original analytical solution to estimate time variable fluxes from the amplitude  
73 damping and the phase shifting, both contained in the temperature signal over depth. Keery et al.  
74 [2007] calculated streambed vertical fluxes using the amplitude damping feature of the  
75 temperature-depth record. They extracted the daily sinusoidal component from noisy field  
76 records using Dynamic Harmonic Regression (DHR) [Young et al., 1999; Taylor et al., 2007].  
77 McCallum et al. [2012] recombined the two sinusoid features, amplitude and phase, to arrive at  
78 two unknowns, streambed thermal diffusivity and advective thermal velocity. Luce et al. [2013]  
79 revisited the original differential equation and combined the information contained in amplitude  
80 and phase to derive explicit analytical solutions for sensor spacing or streambed thermal

81 diffusivity as well as advective thermal velocity. These papers contain a wealth of methods that  
82 can be readily applied to estimate streambed thermal regimes and vertical water fluxes.

83 Further investigated were the impact of parameter uncertainty and non-ideal conditions (such as  
84 sediment heterogeneity and a 2D flow field) on the flux results [Lautz, 2010; Shanafield et al.,  
85 2011; Roshan et al., 2012; Cuthbert and Mackay, 2013; Irvine et al., 2015]. The increasing  
86 popularity of analytical heat tracing methods has led to the development of algorithms that  
87 automate the flux quantification from temperature records, namely *Ex-Stream* [Swanson and  
88 Cardenas, 2011] and *VFLUX* [Gordon et al., 2012]. These methods are implicitly geared towards  
89 quantifying flux time series.

90 What is often overlooked or implicitly assumed in papers that apply methods to quantify fluxes  
91 and thermal diffusivities from field temperature records is the fact that the original analytical  
92 solution is based on the assumption of steady-state flow. This assumption is in contrast to the  
93 aim of understanding natural processes that are commonly transient in nature. While Lautz  
94 [2012] experimented in the laboratory with transient fluxes and found that diurnally forced  
95 analytical solutions are able to offer sub-daily fluxes in reasonable agreement with the known  
96 fluxes of the experiments, McCallum et al. [2012] concluded from field studies that rapid  
97 changes in hydraulic forcing (i.e. floods) lead to erroneous fluxes due to violation of the method  
98 assumptions. Furthermore, a reversal in the flux direction, as expected during flood events (e.g.  
99 the nature of the flood hydrograph as well as return flow of bank storage), complicates the  
100 system's thermal response (i.e. memory effect). We suggest that this will lead to potentially  
101 flawed flux estimates when quantified using heat tracing methods based on the assumption of  
102 harmonic temperature data. This scenario and its implications on heat tracing have not been  
103 comprehensively investigated. However, testing the reliability of heat tracing under highly  
104 transient flux scenarios is a crucial prerequisite for its further application in advancing process  
105 understanding.

106 The aim of this paper is to explore how accurately flux transients can be determined with  
107 methods based on harmonic features that are embedded in temperature records (analytical heat  
108 tracing). We systematically test a) the streambed thermal response time to flux transients, and b)  
109 the accuracy of the water flux, thermal diffusivity and sediment scour/deposition time series  
110 inverted with analytical heat tracing. We demonstrate that near-surface sediment has a particular  
111 thermal response time to sudden flux transients, i.e. quantifiable time between flux-related  
112 thermal disturbance and return to stationarity. Further, we distinguish between the basic thermal  
113 response to a harmonic driver and impacts caused by extraction of fixed-frequency harmonic

114 components that stem from general non-stationarity and transients in vertical fluxes, including  
 115 reversals. Finally, we provide guidance under which conditions the quantification of time-  
 116 variable water flux, thermal diffusivity or sediment scour/deposition from temperature records in  
 117 combination with diurnally forced analytical solutions are reliable. Our results are generic and  
 118 could be useful to other areas of geophysics that utilize time-frequency transformation or  
 119 amplitude and phase extraction of periodically fluctuating signals to quantify natural processes  
 120 or properties.

## 121 2. Methodology

### 122 2.1. Harmonically forced analytical solutions

123 This investigation is based on the 1D conductive-convective heat transport equation which is  
 124 discussed in detail in a number of papers [e.g., Suzuki, 1960; Stallman, 1965; Anderson, 2005;  
 125 Constantz, 2008; Rau et al., 2014] and it will therefore not be stated here again. Rather, we focus  
 126 on the analytical methods derived from the original solution by Suzuki [1960] and Stallman  
 127 [1965]. An analytical solution for the propagation of a harmonic temperature signal with depth is  
 128 given as [Goto et al., 2005]

$$129 \quad (1) \quad T(z, t) = \sum_{i=1}^n A_i \cdot \exp\left(\frac{v_i z}{2D} - \frac{z}{2D} \sqrt{\frac{\alpha_i + v_i^2}{2}}\right) \cdot \cos\left(\frac{2\pi}{P_i} t - \frac{z}{2D} \sqrt{\frac{\alpha_i - v_i^2}{2}}\right)$$

130 where

$$131 \quad (2) \quad \alpha_i = \sqrt{v_i^4 \left(1 + \left(\frac{8\pi D}{P_i v_i^2}\right)^2\right)}.$$

132 Here,  $T$  is the temperature in the sediment at depth  $z$  [L] below the surface, and  $t$  [T] is the  
 133 time. The subscript  $i$  represents individual harmonic frequency components with a total of  $n$   
 134 components.  $A_i$  is the temperature amplitude [K], and  $P_i$  is the period [T] of the harmonic  
 135 component  $i$  (frequency  $f = 1/P$  or angular frequency  $\omega = 2\pi/P$ ). The parameter of interest  
 136 is the 'advective thermal velocity'  $v_i$  [L/T], as it is proportional to the vertical flux (see further  
 137 below).  $D$  [L<sup>2</sup>/T] is the effective thermal diffusivity but without the influence of thermal  
 138 dispersivity as this has been found insignificant for fluxes smaller than  $\sim 10$  m/d [Rau et al.,  
 139 2012a]. However, Rau et al. [2012b] reported that  $D$  can be underestimated due to additional  
 140 thermal spread originating from transverse temperature gradients when the solution requires the  
 141 dimensionality to be reduced to 1-D, even in materials that are considered homogeneous.

142 Equation 1 follows the principle of superposition (Fourier's theorem), which is inherent to the  
 143 linear heat transport differential equation, and allows isolation of the signal's different sinusoidal  
 144 components [Goto et al., 2005].

145 The following reviews and summarizes the general approach that is used to quantify vertical  
 146 fluxes using Equation 1. Options for extracting amplitude and phase of the diel temperature  
 147 harmonic from noisy temperature time series with different signal processing methods will be  
 148 discussed later. The advantage of a harmonic signal is that it has two distinct features, amplitude  
 149 and phase, which allows solving for two unknowns. For a pair of temperature sensors located at  
 150 different depths ( $z$  positive upwards, negative downwards,  $z_2 < z_1$ ) the temperature amplitude  
 151 ratio  $A_r$  and phase shift  $\Delta\phi$  (in radians or days) are defined as [Stallman, 1965; Hatch et al.,  
 152 2006]

$$153 \quad (3) \quad A_r = \frac{A_2}{A_1}$$

$$154 \quad (4) \quad \Delta\phi = \phi_2 - \phi_1$$

155 Stallman [1965] reported that the sinusoidal temperature signal dampens and shifts phase over  
 156 depth (Figure 1).

157 Hatch et al. [2006] used both features, amplitude ratio and phase shift, separately to solve for the  
 158 vertical advective thermal velocity

$$159 \quad (5) \quad v_{t,Ar} = \frac{2D}{\Delta z} \ln(A_r) + \sqrt{\frac{\alpha + v_{t,Ar}^2}{2}}$$

$$160 \quad (6) \quad v_{t,\Delta\phi} = \sqrt{\alpha - 2 \left( \frac{4\Delta\phi\pi D}{P\Delta z} \right)^2}$$

161 When using Equations 5-6 the disadvantage is that the thermal diffusivity must be known before  
 162 calculating velocities as it significantly influences the results [Hatch et al., 2010]. Equations 5-6  
 163 were field tested and results by the two equations were found to differ significantly from each  
 164 other despite relying on the same thermal parameters [Rau et al., 2010].

165 Luce et al. [2013] revisited Stallman's [1965] original solution and found that amplitude and  
 166 phase can be combined and expressed as dimensionless velocity as

$$167 \quad (7) \quad \eta = -\frac{\ln(A_r)}{\Delta\phi}.$$

168 The combined information in Equation 7 is the ratio between the advective ( $v_t$ ) and the  
 169 diffusive ( $v_d$ ) thermal velocity, as

$$170 \quad (8) \quad v^* = \frac{v_t}{v_d} = \frac{1-\eta^2}{\sqrt{2\eta(1+\eta^2)}} = \frac{Pe}{2}.$$

171 Conveniently,  $Pe$  is the thermal Péclet number indicating dominance of diffusive ( $Pe < 1$ ) or  
 172 convective conditions ( $Pe > 1$ ). Equation 7 is useful to determine the direction and change of  
 173 water velocity simply from temperature amplitude and phase information without any further  
 174 parameters, such as sensor spacing or thermal diffusivity [Luce et al., 2013].

175 The damping depth  $z_d$  of the sinusoid is determined as [Goto et al., 2005; Luce et al., 2013]

$$176 \quad (9) \quad z_d = \sqrt{\frac{DP}{\pi}}.$$

177 This is the depth at which the temperature amplitude is damped to 1/e of its original value.  
 178 Assuming a constant sensor spacing ( $\Delta z$ ), the thermal diffusivity can be calculated using [Luce  
 179 et al., 2013]

$$180 \quad (10) \quad D = \frac{2\pi\eta\Delta z^2}{P(\ln^2(A_r) + \Delta z^2)}$$

181 It is noteworthy that results from this equation are equivalent to that published by McCallum et  
 182 al. [2012]. They reported that the thermal diffusivity calculated using field data can exceed  
 183 physically possible values during periods when the stream stage rapidly changes (transient flux  
 184 conditions). While they suggested that the method may break down during such conditions, they  
 185 did not investigate its limitations in correctly resolving parameters over the duration of transient  
 186 conditions.

187 Analogously, assuming a constant thermal diffusivity ( $D$ ), the sensor spacing ( $\Delta z$ ) is  
 188 determined as [Luce et al., 2013; Tonina et al., 2014]

$$189 \quad (11) \quad \Delta z = z_d \sqrt{\frac{\ln^2(A_r) + \Delta \phi^2}{2\eta}}$$

190 Interestingly, Luce et al. [2013] and Tonina et al. [2014] have used this to quantify sediment  
 191 scour/depositional processes, indicated by a time variable sensor spacing, based on field data  
 192 obtained during a period of transient stream discharge. However, they did not consider the



193 possible limitations that transient fluxes can impose on methods based on the diurnal heat  
 194 forcing. Here, it is important to note that equations 10 and 11 are exactly the same and can either  
 195 quantify sediment thermal diffusivity ( $D$ ) or scour/depositional processes inferred from sensor  
 196 spacing ( $\Delta z$ ).

197 Finally, the advective thermal velocity is determined using [Luce et al., 2013]

$$198 \quad (12) \quad v_t = \frac{2\pi\Delta z(1-\eta^2)}{P\sqrt{(1+\eta^2)(\ln^2(A_r) + \Delta z^2)}}.$$

199 Equation 13 is the final step to quantify the Darcy flux ( $q$ ) from advective thermal velocity as

$$200 \quad (13) \quad q = \left( \varepsilon + (1-\varepsilon)\frac{c_s^v}{c_w^v} \right) v_t$$

201 where additional sediment properties are required:  $\varepsilon$  is the porosity of the sediment,  $c_s^v$  and  $c_w^v$   
 202 are the volumetric heat capacities of the solids and water, respectively. Equation 13 is stated here  
 203 for sake of completeness, but will not be used further to quantify the Darcy flux, since this is not  
 204 the aim of the paper. Instead, we let the advective thermal velocity,  $v_t$ , represent the convective  
 205 conditions (vertical flux magnitude and direction). In this paper we use Equations 3-12 to invert  
 206 fluxes from temperature data that has been generated by a numerical model described in the next  
 207 section.

## 208 **2.2. Numerical modeling**

209 In this paper a transient numerical model was used to generate the thermal response  $T(z,t)$  to  
 210 step and ramp changes in the water velocity (i.e. worst case transient scenario). The conceptual  
 211 model is a diurnally forced water saturated near-surface system (i.e. like a streambed). The  
 212 approach is an analogue to any real-world transient flux signal, as this can be thought of as  
 213 multiple discrete-time steps with variable magnitudes and durations.

214 COMSOL Multiphysics V5 [COMSOL, 2014] was used as the numerical solver for the  
 215 conductive-convective heat transport equation in a one-dimensional domain, resembling the  
 216 vertical extent of a near-surface hydrologic system. For all simulations a sinusoidal temperature  
 217 signal with period  $P = 1$  day and amplitude of  $3^\circ\text{C}$  at a mean of  $20^\circ\text{C}$  was applied at the top of  
 218 the domain. The bottom of the domain was held at a constant temperature of  $20^\circ\text{C}$  at a large  
 219 enough distance (30 m) to have no further effect on the simulated temperatures in the upper 1 m

220 used in the analysis. The initial condition was  $T = 20\text{ }^{\circ}\text{C}$  across the whole model domain. The  
221 mesh increased in size from 4 mm at the upper boundary to 1 cm at the base of the domain. The  
222 absolute solver tolerance was set to  $1 \cdot 10^{-5}\text{ }^{\circ}\text{C}$  with a relative tolerance of  $1 \cdot 10^{-9}$ , small enough  
223 to ensure that the model output was no longer sensitive to changes in these values. The  
224 numerical models were accurate to within  $\sim 0.0001\text{ }^{\circ}\text{C}$  against the range of analytical models  
225 during steady velocity periods.

226 Each simulation was conducted for a total time of 30 days with a constant advective thermal  
227 velocity assigned to the first 10 days, followed by a step change in advective thermal velocity  
228 and another 20 days of simulation. Temperature records were generated at 96 time steps per day  
229 (15 min time step) at the top boundary and at the depths: 0.02 m, 0.05 m, 0.1 m, 0.2 m, 0.3 m,  
230 0.5 m, 0.75 m and 1 m (see dashed horizontal lines in Figure 1). The large number of depths  
231 allowed investigation of both up- and downward flow by evaluating data from sensor locations  
232 at depths where the temperature signal was not damped beyond recognition (temperature  
233 variations well above the limits of typical field instrument resolution, typically  $0.001\text{-}0.01\text{ }^{\circ}\text{C}$ ).

234 The following transient advective thermal velocity scenarios were simulated in separate sub  
235 cases:

- 236 1. 0 m/d followed by a downward step change: -0.01, -0.1, -0.5, -1 and -5 m/d,
- 237 2. 0 m/d followed by an upward step change: 0.01, 0.1, 0.5, 1 and 2 m/d,
- 238 3. Reversal step change from -1 m/d downwards to 1 m/d upwards, and from 1 m/d  
239 upwards to -1 m/d downwards,
- 240 4. Linear increase from 0 to -1 m/d within a time of 0.5, 1, 2 and 4 days.

241 The velocity reversals are particularly interesting as the thermal signal is transported downwards  
242 and then upwards (or vice versa) by the water flux by convection while conducting  
243 simultaneously depending on the temperature-depth gradient. The linear streambed velocity  
244 increases represent the likely responses to different hydrograph characteristics, for example fast  
245 flux transient caused by flash flooding, or slow flux transients due to snow melt.

246 To illustrate the influence of the thermal diffusivity on the results, all cases were simulated for  
247 physically realistic minimum and a maximum thermal diffusivity as reported in the literature  
248 [i.e., Shanafield et al., 2011; McCallum et al, 2012]. The numerically simulated temperature time  
249 series were first processed using different signal extraction methods, and then Equations 3-12  
250 were used to invert for time series of transient velocities and thermal diffusivities. To provide  
251 quantifiable measures of the suitability of heat tracing during transient velocities we calculate

252 the maximum error and the root-mean-square error (RMSE) between the modeled and inverted  
253 advective thermal velocity and diffusivity data. Finally, we test how well signal processing  
254 techniques can distinguish between temperature signal non-stationarity caused by flux transients  
255 and other processes by repeating the first set of model simulations with a previously measured  
256 and published temperature record [Rau et al., 2010] as the upper boundary.

### 257 **2.3. Extraction of harmonic amplitudes and phases from temperature records**

258 A prerequisite to the calculation of water flux and thermal diffusivity are temperature time series  
259 measured by sensors in at least two different depths of the water-saturated sediment. From these  
260 measurements the strongest frequency component, the daily frequency [Stallman, 1965; Hatch et  
261 al., 2006; Keery et al., 2007], is commonly extracted. Here, we evaluate the capability and  
262 accuracy of the four most commonly used signal processing techniques that offer time-  
263 dependent amplitude and phase extraction. To obtain amplitude and phase data from the  
264 sinusoidal component embedded in typically noisy field data a transformation of data from the  
265 time domain into the frequency domain is needed.

#### 266 **2.3.1. Harmonic peak identification**

267 As a benchmark for the results obtained from different signal processing methods the peak  
268 amplitudes and timings were directly identified from the model output. This is only appropriate  
269 when the signal consists of a single harmonic frequency as was required by Equations 3-12 and  
270 as used for the numerical model. The sampling frequency will limit how accurately peaks  
271 (minima and maxima) can be determined. This means that amplitudes and phases may not be  
272 optimally detected as any particular minima or maxima may not occur exactly at the sampling  
273 time. We apply an algorithm that uses the neighboring values around the peaks to find the exact  
274 magnitude and timing with 2<sup>nd</sup> order polynomial regression. This approach results in a best  
275 possible peak time-resolution offering 2 samples per day for peaks. We refer to this approach as  
276 “peak picking”.

#### 277 **2.3.2. Windowed Fourier Transform (WFT)**

278 The most obvious method is the discrete Fourier transform (DFT) and its computational  
279 representation, the fast Fourier transform (FFT). A common approach to obtain frequency  
280 information is to apply the FFT to a fixed time window that is shifted along the complete record  
281 resulting in the windowed Fourier transform (WFT). This approach was suggested by Keery and  
282 Binley [2007] and successfully used by Cuthbert et al. [2011].

283 WFT offers the advantage of being able to identify signal non-stationarity, as a measure of  
284 transient fluxes, in the time domain. However, it is well known that the WFT has a constant  
285 frequency resolution due to the fact that the window size used in the time domain defines the  
286 resolution in the frequency domain [Oppenheim and Schaffer, 1989]. This means that the window  
287 size must have an appropriate amount of samples so that the frequency resolution can capture  
288 information at 1 cpd. This amounts to window sizes that are multiples of samples per day (one  
289 cycle based on daily fluctuations). Further, the minimum window size must be one harmonic  
290 cycle in the time domain as otherwise the discrete samples in the frequency domain do not  
291 coincide with the desired frequency. While increasing the window size will reduce the artifacts  
292 from spectral leakage, this will also diminish the ability to accurately detect the exact timing of  
293 changes in the water flux. Since the focus is on determining transient fluxes the minimum  
294 window size, a 1 day window with 96 samples (for our sampling interval of 15 min), was used.  
295 To maximize the frequency-time information the window was continuously shifted by 1 sample  
296 at a time. This approach is equivalent to a moving rectangular window. While different window  
297 shapes will change the extracted amplitude-phase relationship, we focus on avoiding any side  
298 effects arising from window functions. The amplitude and phase information, given as the length  
299 and angle of the complex FFT output, were assigned to the midpoint of the time window.  
300 Amplitudes and phases were then used to quantify fluxes and thermal diffusivities with  
301 Equations 3-6, 10 and 12.

### 302 **2.3.3. Zero-phase (forward-backward) filtering**

303 A slightly different amplitude and frequency extraction technique was suggested by Hatch et al.  
304 [2006]. Their attempt of recovering the full daily harmonic component in the time domain  
305 deployed a windowed filter. The first step is similar to that previously explained for WFT, but  
306 then the frequency spectrum is multiplied with a band-pass window centered on 1 cpd to retain  
307 the daily frequency and cancel the lower and higher components. This is equivalent to a time-  
308 domain convolution of the signal and filter kernel but is often computationally easier. This 1 cpd  
309 frequency record is subsequently inverted back to the time domain. Here, the choice of window  
310 will have an effect on the spectral leakage, and the *Tukey* window was suggested because it  
311 provides an optimization between maintaining the gain for the desired frequency and optimizing  
312 the fade of side-band components [Harris, 1978]. The window size (filter order) must be  
313 multiples of days to allow accurate sampling of the 1 cpd frequency. Since manipulating the  
314 amplitude information in the frequency domain will inevitably also modify the phase  
315 information, a forward-backward filter (e.g., Matlab's *filtfilt* function implemented in the Signal

316 Processing Toolbox) must be deployed to allow an exact cancelation of the phase error  
317 introduced when filtering in the forward direction only [Hatch et al., 2006].

318 Again, while an increasing window size will result in increasing filter stability it also reduces the  
319 temporal resolution (i.e. makes it harder to accurately identify flux transients). A minimum filter  
320 order of 384 (= 4 days at 15 min sampling intervals) was determined to result in a stable time-  
321 domain output. The filter output in the time domain must undergo “peak picking” before fluxes  
322 can be calculated [Hatch et al., 2006].

#### 323 **2.3.4. Continuous Wavelet Transform (CWT)**

324 One significant limitation of the Fourier transform is the Heisenberg–Gabor limit, the  
325 relationship between resolution in frequency and time domain [Havin and Jöricke, 1994].  
326 However, time-varying amplitude and phase information, as measured for time-varying flux and  
327 thermal diffusivity, implies that the signal is non-stationary. The continuous wavelet transform  
328 (CWT) appears to be better suited for extracting time-variant frequency domain features from  
329 temperature records. Onderka et al. [2013] successfully tested the application of CWT in  
330 analytical heat tracing. Pidlisecky and Knight [2011] use CWT to derive infiltration rates from  
331 1-D resistivity records. For a useful practical guide to the CWT the interested reader is referred  
332 to Torrence and Compo [1998]. Further, Grinsted et al. [2004] offer an excellent practical  
333 overview of the wavelet transforms and its application to geophysical time-series.

334 Here, we adopt the same approach as was deployed by Onderka et al. [2013] using the *Morlet*  
335 mother wavelet because of its close alignment with the harmonic waveform. In the time domain  
336 this wavelet is a superposition of a harmonic and the Gauss function with maximum weight  
337 given to the center of the window in the time domain. The wavelet can be stretched or  
338 compressed depending on the desired frequency to be analyzed. We used the CWT implemented  
339 in Matlab by Erickson [2014].

#### 340 **2.3.5. Dynamic Harmonic Regression (DHR)**

341 Keery et al. [2007] used Dynamic Harmonic Regression (DHR) to extract the diel harmonic  
342 from discrete-time temperature records measured at multiple depths in the sediment. DHR was  
343 developed by Young et al. [1999] as an extension to Fourier analysis that is particularly suitable  
344 for non-stationary signals. The technique is a data based mechanistic approach that features  
345 time-variable spectral coefficients that estimate signal amplitude and phase information [Vogt et  
346 al., 2010]. DHR is readily implemented in Matlab as the CAPTAIN toolbox [Taylor et al., 2007]  
347 and is a state-of-art choice of filter for a non-stationary signal [Young et al., 1999]. For best

348 compatibility with recent research we implemented DHR in the same way as Keery et al. [2007],  
349 Vogt et al. [2010] and in VFLUX [Gordon et al., 2012]. The reader is therefore referred to these  
350 papers for further details. Noteworthy is the recommendation for an optimum sampling  
351 frequency of 12 samples per day, as over- and under-sampling can cause incorrect signal  
352 identification by the DHR algorithm [Gordon et al., 2012].

### 353 3. Results and discussion

#### 354 3.1. Properties of field temperature records and the harmonically-forced analytical 355 solution

356 As a first point it is vital to consider the characteristics of temperature signals measured in  
357 sediments. It is apparent from a number of existing studies that the temperature signal is  
358 dominated by the diel and, if the record is long enough, annual frequency [i.e., Hatch et al.,  
359 2006; Keery et al., 2007; Wörman et al., 2012]. However, the record typically contains other  
360 frequency components that are often referred to as noise. The annual and diel components are  
361 controlled by the continuous celestial movements, and thus can be considered harmonics with  
362 precisely known cycles (e.g.,  $P_{diel} = 86,400$  s). More complicated to determine are the “noisy”  
363 components which will depend on various natural factors, for example the local climate, site and  
364 seasonal specific details (i.e. shading) and sensor noise.

365 The Fourier Theorem stipulates that a continuous function can be decomposed into an infinite  
366 series of individual harmonics with different amplitudes and phases. In practice, temperature  
367 measurements are recorded digitally as discrete samples in time. Therefore, the signal can be  
368 decomposed into a finite series of harmonics using the Discrete Fourier Transform (DFT).  
369 However, it is important to consider that each of the components identified by the DFT is a  
370 stationary harmonic, and that the resolution in the time domain will also determine the frequency  
371 domain resolution [Oppenheim and Schaffer, 1989].

372 Also noteworthy here is the fact that the differential heat transport equation is of linear nature.  
373 This means that the sediment depth response to any temperature signal at the surface is the sum  
374 of the individual harmonics that form part of the original signal, but each weighted according to  
375 Equation 1 [Goto et al., 2005]. Importantly, the weighting depends on the signal frequency ( $f = 1/P$ , note  $P_i$  in Equation 1) and the water flux, which translates into exponentially damped  
376 amplitudes and linearly shifted phases (Figure 1). In other words, the water flux modulates the  
377 depth propagation of harmonics. Quantifying the vertical flux from the properties of individual  
378 harmonics, i.e. using the amplitude damping and phase shifting, is exactly what heat tracing  
379 methods intend to achieve. In essence, the sediment acts as a frequency filter where faster  
380 frequencies are damped quicker and slower frequencies propagate further as a function of the  
381 vertical flux [Hatch et al., 2006]. This phenomenon has been exploited to calculate thermal  
382 diffusivity and a steady-state vertical flux from temperature spectra [Wörman et al., 2012]. It is  
383 clear that diel amplitudes and phases cannot simply be selected from unfiltered temperature  
384

385 records, as has been previously done [Fanelli and Lautz, 2008; Lautz, 2010], because the “noise”  
386 which consists of inherently different frequencies distorts the diel signal in a depth and flux  
387 dependent way. Extraction of amplitude and phase information with signal processing  
388 techniques is therefore a crucial component of heat tracing with diurnally forced analytical  
389 solutions.

390 In the context of heat tracing it is important to remember that stationary signals require that their  
391 statistical properties – here, the features describing a sinusoidal wave – do not change over time  
392 [Oppenheim and Schaffer, 1989]. When this is considered in relation to Equation 1, it becomes  
393 clear that when a hypothetically stationary temperature harmonic (i.e., a temperature sinusoid at  
394 the upper boundary) propagates over depth its stationarity is maintained only if the vertical water  
395 flux is in steady-state ( $v_t = \text{const}$  in Equation 1). Importantly, any transients in the water flux  
396 (advective thermal velocity  $v_t = f(t)$  in Equation 1) will transform a previously stationary  
397 harmonic into a non-stationary signal. Figure 2 illustrates this point using a step change in the  
398 water flux as a worst case transient for a pure harmonic (a) and actual temperature (b) data  
399 obtained from Rau et al. [2010]. In essence, any flux transient, equivalent to a time-change in the  
400 advective thermal velocity ( $v_t$ ) in Equation 1, will influence the stationarity of the temperature-  
401 time signal (see also Figure 1) and thus add to any existing non-stationary features already  
402 embedded in the temperature signal (Figure 2b).

403 In reality many field studies that develop and apply analytical heat tracing to gain  
404 hydrogeological process understanding are interested in the changes in water flux over time. In  
405 other words, they rely on the fact that the analytical heat tracing can detect flux transients [e.g.,  
406 Hatch et al., 2006; Keery et al., 2007; Lautz et al., 2010; Rau et al., 2010; Swanson and  
407 Cardenas, 2010; Vogt et al., 2010; Jensen and Engesgaard, 2011; Munz et al., 2011; McCallum  
408 et al., 2012; Luce et al., 2013; McCallum et al., 2014; Tonina et al., 2014; Gariglio et al., 2014].  
409 Here, we test whether flux transients can be quantified using analytical methods and determine  
410 their behavior when the temperature signal becomes non-stationary caused by transient fluxes.  
411 From a signal processing perspective it is useful to investigate how accurately the onset of  
412 sudden signal non-stationarity can be delineated and attributed to a cause, such as changes in the  
413 water flux implicitly expressed in the temperature records.



### 414 3.2. System response to sudden water flux transients

415 It is important to understand the thermal modulation of transient fluxes before proceeding with  
416 the analysis of signal amplitude and phase extraction methods, and their subsequent impact on  
417 the quantification of thermal diffusivities or sediment scour/deposition and the temporal fluxes.  
418 This provides the foundation for a quantitative assessment of the possible artifacts that signal  
419 processing imposes on the physical processes contained within temperature harmonics.

420 How long does it take for a harmonic temperature signal to return to stationarity when affected  
421 by a sudden change in flux, e.g. a step change? Figure 3a shows the sediment thermal response  
422 to sudden advective thermal velocity transients. This is defined as the difference between the  
423 numerically modeled temperature response to a velocity step change and the stationary  
424 temperature signals that were calculated with Equations 1-2 for the two different steady-state  
425 velocities that the step consists of. The thermal response is shown for two different depths and a  
426 minimum, average and maximum thermal diffusivity (as was used by Shanafield et al. [2011]  
427 and McCallum et al. [2012]). After an initial temperature jump (sharp non-stationarity) caused  
428 by the velocity step it is clear that the underlying thermal response resembles the characteristic  
429 exponential relaxation described by the generic equation  $\exp(-t/\tau)$ , where  $\tau$  is the response  
430 time [T]. The magnitude of the temperature non-stationarity induced by the velocity step  
431 decreases from approx. 2.3 °C to 0.2 °C (for a boundary amplitude of 3 °C) with increasing  
432 thermal diffusivity (Figure 3a). The relaxation time  $\tau$  for  $D_{avg} = 0.075 \text{ m}^2/\text{d}$  is approx. 0.15  
433 days, but this depends on the speed of propagation (velocity magnitude and depth of  
434 measurement) and the sediment thermal diffusivity. Figure 3a reveals that the minimum thermal  
435 diffusivity causes the largest initial temperature jump but also the shortest thermal response time  
436 (~0.04 days for a spacing of 0.1 m).

437 Not surprisingly, the sediment thermal response will also depend on the timing of the velocity  
438 transient in relation to the phase of the upper harmonic temperature boundary. Figure 3b shows  
439 an example of the velocity step change with the onset occurring at 8 different times shifted by  
440 0.125 days ( $\pi/4$  for  $f = 1$  cpd). Again, the sediment thermal response at depth was calculated  
441 as the difference between the temperature output from the numerical model and the analytical  
442 solution. Interestingly, the magnitude of the thermal response ranges between ~0.1 °C and 1.4 °C  
443 for the step at 0.125 d and 0.375 d, respectively, and with shape of the sediment thermal  
444 response suggesting a more complex function compared to just an exponential relaxation.  
445 Nevertheless, the perturbation decays over time as expected.

446 In summary, a water flux step change causes a sudden propagation of non-stationarity in the  
447 temperature signal over depth followed by gradual return to stationarity over time. This is due to  
448 the previously stationary temperature-depth harmonic being moved downwards or upwards by  
449 the sudden change in water flux before stationarity is reached again. For the velocity used in this  
450 example and for realistic thermal diffusivities ( $0.02 < D < 0.13 \text{ m}^2/\text{d}$ ) the sediment response  
451 time is  $0.04 < \tau < 0.24$  days. Importantly, it is evident that the temperature non-stationarity  
452 caused by a worst-case transient velocity (step change) diminishes within one harmonic cycle (1  
453 day).

### 454 **3.3. How do different signal extraction methods perform when the signal is non-** 455 **stationary?**

456 Figure 2b suggests that the temperature non-stationarity caused by a transient water flux is  
457 superimposed on temperature signal non-stationarities caused by other factors (see earlier  
458 discussion). While the importance of correctly extracting amplitudes and phases was established  
459 earlier, it is vital to reveal how different signal extraction techniques respond to non-stationarity  
460 caused by only the transient water flux, since these transients are of main interest. Hatch et al.  
461 [2006] discussed the possible impact of signal filter edge effects on the fluxes and suggested that  
462 the effect of filtering should be further investigated. While different authors have used various  
463 different signal processing techniques [Hatch et al., 2006; Keery et al., 2007; Cuthbert et al.,  
464 2011; Onderka et al., 2013], their impact on the flux results have mostly been assumed  
465 negligible, and were neither comprehensively investigated nor quantified.

466 Here, we raise the question: How accurate are different signal processing techniques in  
467 delineating non-stationary harmonic features (e.g. amplitudes and phases) caused by transient  
468 fluxes when they are buried in a “noisy” signal? This can be answered by comparing the  
469 response of signal extraction techniques to a sudden non-stationarity. Figure 4 illustrates the  
470 response of four different signal processing techniques (WFT, filtfilt, CWT and DHR; see  
471 methods section for details) to the non-stationarity of an otherwise harmonic temperature signal  
472 caused by a step change in advective thermal velocity. Figures 4a, 4c, 4e, 4g show the extracted  
473 amplitudes and 4b, 4d, 4f, 4h the phases at different depths with time relative to the non-  
474 stationarity. Since both amplitude and phase are combined to invert the vertical velocity and  
475 thermal diffusivity (see Equations 7-12) it is essential to inspect both separately.

476 Figure 4 demonstrates the following features:

- 477 ■ The four signal processing techniques demonstrate different responses to non-stationarity

- 478   ▪ While the extracted signal amplitudes are generally smooth, the phase data can exhibit  
479    significant artifacts, e.g. oscillations (Figure 4b,d,f,h)
- 480   ▪ The response to signal non-stationarity is an erroneous temporal spreading (“smearing”) over  
481    time, with both the amplitude and phase responding before the actual velocity transient has  
482    occurred
- 483   ▪ Significant “smearing” occurs for a minimum of 1 cycle for WFT (Figure 4a,b), and  
484    maximum time of ~3 cycles for filtfilt (Figure 4c,d)
- 485   ▪ The WFT methods shows strong oscillations in particular for phase data where the signal to  
486    noise ratio is low, e.g. for the deepest observation points (Figure 4b)

487 In general, the above observations highlight that signal processing can strongly impact the  
488 quantification of vertical fluxes and thermal diffusivities during transient changes.

### 489       **3.4. Quantification of transient fluxes and thermal diffusivities**

490 The previously presented amplitude and phase data (Figure 4) were used to derive amplitude  
491 ratios (Equation 3) and phase shifts (Equation 4) based on two observation points located at  
492 different depths. Then, the velocities and thermal diffusivities were quantified from Equations 7-  
493 12 and compared with those used as input to the numerical model. This was done with amplitude  
494 and phase data extracted using all four signal processing techniques (Figure 4). Figure 5  
495 summarizes the vertical velocities (a, c, e, g) and thermal diffusivities (b, d, f, h) for different  
496 velocity step changes, 0 to -1 m/d (a & b), 0 to 1 m/d (c & d), reversal from -1 m/d to 1 m/d (e &  
497 f) and reversal from 1 m/d to -1 m/d (g & h). As a best-case benchmark the results from picking  
498 amplitudes and phases straight from the simulated temperature data (which is possible in this  
499 case since a sinusoidal temperature boundary is used), are also shown. We emphasize that this  
500 approach presents the best possible time resolution that can be achieved from methods that rely  
501 on a harmonic signal, as a sinusoid only has 2 features per cycle (amplitudes and phases at  
502 maximum and minimum).

503 Figure 5 shows significant artifacts in vertical velocities and thermal diffusivities that stem from  
504 quantifying the heat tracing derived velocity over a step change in the modeled water velocity.  
505 Best results are achieved when peak picking is applied to unfiltered harmonic temperature data  
506 (red squares in Figure 5) showing only a small deviation from the modeled velocity. The errors  
507 between modeled and inverted velocity are caused by the streambed’s non-stationary thermal  
508 response, as was discussed earlier (Section 3.2, Figure 3). However, this approach can only be

509 used when the temperature signal is a pure harmonic (stationary) and must not be applied to  
510 noisy real-field measurements.

511 Being deduced from the previously shown amplitude and phase data (Figure 4) the velocity and  
512 diffusivity results are also “smeared” across ~4-5 cycles, approximately centered at the time at  
513 which the transient velocity occurred (Figure 5). It is noteworthy that for downward velocity  
514 steps the thermal diffusivity is overestimated, and it is underestimated for upward velocity steps.  
515 Note that sensor spacing (Equation 11) is prone to the same anomaly because it originates from  
516 reformulating the thermal diffusivity (Equation 10). Figures 6 and 7 show the same calculation  
517 for different velocity step sizes in both directions and found that the response becomes  
518 increasingly smeared and delayed for large velocity steps. Interestingly, the results in Figures 5,  
519 6 and 7 also indicate that for velocity steps up to  $\pm 1$  m/d the “smearing” is independent of either  
520 the velocity step magnitude or direction, even for velocity reversals. Further, results show that  
521 for velocity transients exceeding -5 m/d (Figure 6) and 2 m/d (Figure 7) the response shifts  
522 forward in time and the error between modeled and inverted advective velocity increases  
523 significantly.

524 These results demonstrate that signal processing techniques, and not the assumption of steady-  
525 state flux inherent to the analytical solution (Equation 1), is the culprit responsible for inaccurate  
526 detection of transient fluxes quantified from harmonically forced analytical solutions. This is due  
527 to the uncertainty principle (Heisenberg-Gabor limit) based on fixed resolution in both time and  
528 frequency domain inherent to any signal filtering that relies on the Fourier transform [Havin and  
529 Jöricke, 1994].

530 While the scenarios presented in Figures 5-7 resemble a worst case caused by highly transient  
531 hydrographs (e.g. flash floods, dam releases), streams that are dominated by snowmelt typically  
532 experience slower flux transients. Figure 8 shows the response of heat tracing to different rates  
533 of velocity change (an analogue of the hydrograph slope assuming no change of hydraulic  
534 conductivity over time) modeled as a linear increase of the advective thermal velocity from 0 to -  
535 1 m/d within 0.5, 1, 2 and 4 days. A summary of the match between modeled and inverted  
536 advective thermal velocities and diffusivities can be found in Tables 1 and 2, respectively, for  
537 the four different filtering methods and the four different rates of velocity change (Figure 8) as  
538 well as the step change (first row in Figure 5). Here, it is interesting to note that the velocities  
539 inverted without applying any signal processing methods directly from the temperature  
540 amplitudes and phases (red markers) in all cases closely resemble the actual velocities used to  
541 drive the numerical model (Figure 8 first column, RMSE < 0.031 °C in all cases). In contrast

542 inverted thermal diffusivities (or sensor spacing) are more sensitive to flux transients, with  
543 values generally underestimated and with decreasing errors for a decreasing rate of velocity  
544 change (Figure 8 second column). The time decay of the error is in agreement with the  
545 streambed thermal response evaluated in Figure 3.

546 Figure 8 further illustrates the capability of the different signal processing methods to delineate  
547 different degrees of signal non-stationarity. As expected, the less transient the better the response  
548 of signal processing methods, indicated by the degree of matching between modeled and  
549 inverted velocity (decreasing RMSE in Table 1). It is apparent that DHR is the overall best  
550 performing (most time-variant) method with inverted and modeled velocities matching the  
551 closest (smallest RMSE in Tables 1 and 2). By contrast, CWT shows the slowest response to  
552 velocity transients (highest RMSE in Tables 1 and 2). Interestingly, thermal diffusivities inverted  
553 after applying the signal processing methods are consistently overestimated during the velocity  
554 transient. Further, it is noteworthy that there remains a significant error in the inverted velocities  
555 (max. 0.06 m/d for DHR) and diffusivities for a velocity ramp that spans 4 harmonic cycles. This  
556 proves that heat tracing results are increasingly affected by the signal processing methods under  
557 increasing transient advective velocities (see RMSE values in Tables 1 and 2). Sudden flux  
558 transient can cause errors of up to 57 % in velocity (Table 1) and 37 % in thermal diffusivity  
559 (Table 2) estimates even when DHR, the most time-variant spectral filter, is used. Inaccuracies  
560 in the inverted results persist for up to  $\pm 2$  days around the occurrence of sudden flux transients  
561 (Figures 5 and 8). The mildest case of velocity transient studied here (-1 m/d velocity change in  
562 4 days:  $dv/dt = 0.25 \text{ m/d}^2$ ) introduces an error of  $\sim 6$  % in velocity (Table 1) and  $\sim 4$  % in  
563 thermal diffusivity (Table 2) with inaccuracies during  $\pm 1$  days of the start and end of the velocity  
564 change (Figures 8 and first row in Figure 5). These errors are larger for all other signal  
565 processing methods and rates of velocity change studied.

566 McCallum et al. [2012] have reported spurious thermal diffusivities in their field investigation  
567 during highly transient flow conditions, e.g. dam releases and floods. Further, they found that  
568 water flux calculated by heat tracing reacted before the change in hydraulic gradients. Both  
569 observations are consistent with the erroneous delineation of transient fluxes caused by signal  
570 processing as illustrated in this paper (see Figures 5 and 6). It has previously been suggested that  
571 sub-cycle resolution for vertical fluxes can be obtained [Lautz, 2012]. Here, we demonstrate  
572 that, while signal processing techniques offer sub-cycle resolution values for amplitudes and  
573 phases, the smoothing of the inverted fluxes across sudden transients (and oscillations in the case  
574 of phase data) may not resemble the actual transient flux. It is therefore not recommended to

575 trust flux and thermal diffusivity or sediment scour/deposition results during times when fluxes  
576 are expected to be transient (e.g. floods). This suggests that hydraulic head data should be  
577 interpreted together with temperature data in order to assess transient conditions; otherwise the  
578 use of heat tracing based on harmonic signals becomes untrustworthy.

579 The above discussion raises the question as to which signal processing technique performs best  
580 under transient flux conditions. Figure 5 suggests that there is no simple answer, as there appears  
581 to be a trade-off between the distortion of the magnitude and the duration of the flux and  
582 diffusivity estimates. The most suitable approach will depend on the individual circumstances  
583 and whether the focus lies on estimating the magnitude or timing of transient fluxes.

### 584 **3.5. Biased process estimates caused by a non-stationary temperature boundary**

585 While the previous discussion revealed that signal processing techniques hamper the accurate  
586 time-resolution of quantified fluxes and thermal diffusivities or sediment scour/deposition when  
587 the water flux is transient, the influence of non-stationarity in the field temperature records has  
588 so far been neglected but must also be considered. Rau et al. [2010] measured the temperatures  
589 at the bottom of the stream column and at several depths within the streambed sediment with a  
590 sensor spacing of 0.15 m at 3 different horizontal locations within a small perennial stream in  
591 Australia over a 3-month period in 2007. Here, we use a 30-day subset of the uppermost  
592 temperature data from location C (see Rau et al. [2010]) as a real-field boundary condition for  
593 our numerical model. Figure 9a shows the multi-level temperature time series obtained from  
594 numerical modeling using a velocity step change and the measured surface water temperature as  
595 the boundary condition [Rau et al. 2010]. Here, the non-stationarity is present in the system due  
596 to both natural causes (e.g. weather changes, site specific shading, sensor noise, see 3.1 earlier)  
597 and water flux imposed by the flux step. The challenge for the accurate detection of amplitudes  
598 and phases is to maximize the extracted signal induced by the change in the water flux and to  
599 minimize the “noise” with frequencies other than diel in the forcing temperature data.

600 Figures 9b and 9c show vertical velocities and thermal diffusivities quantified with Equations 10  
601 and 12 after applying the different signal processing techniques outlined in the methods section.  
602 The results clearly show that general temperature non-stationarity significantly ‘leaks’ into the  
603 velocity results. The WFT is revealed as the worst performing technique with apparent velocity  
604 variations of similar magnitude to the actual velocity step that is to be identified. This is due to  
605 the shortness of the 1-day window selected to maximize the detection of the timing of the  
606 velocity transients. Increasing the window would increase the method’s accuracy during steady

607 velocity periods, but at the expense of reducing its ability to accurately delineate the step change.  
608 The technique with best performing amplitudes and phase extraction is the zero-phase forward-  
609 backward filter (*filtfilt* in Matlab), originally proposed by Hatch et al. [2006]. However, this  
610 method still smooths the velocity transient (Figure 9b), and produces an apparent jump in  
611 thermal diffusivity (Figure 9c), caused by the window length. By contrast DHR, which has been  
612 attributed with robust detection of harmonics embedded in non-stationary signals [Vogt et al.,  
613 2010; Gordon et al., 2012], exhibits significant noise in our test (Figures 7b and 7c). Our results  
614 confirm what McCallum et al. [2012] had observed in their field application, mainly that heat  
615 tracing results should not be trusted during times when the flux is expected to be transient. We  
616 suggest that thermal diffusivity jumps in field data indicate times when the vertical flux is highly  
617 transient or when erosion-depositional processes occur. However, as both would occur during  
618 transient conditions it would be difficult to disentangle real changes in sensor spacing (as a  
619 proxy for scour/depositional processes) from anomalies induced by transient velocities (Figures  
620 5-8).

621 Figure 9 also demonstrates that there is a lower limit to the detection of velocity changes. This  
622 limit depends on the signal-to-noise ratio, the ratio between temperature signal non-stationarity  
623 caused by the transient water flux and other sources of non-stationarity. Fourier based signal  
624 processing methods are prone to leakage between different frequencies. Leakage can obscure the  
625 harmonic signal of interest, depends on the filter parameters and is difficult to quantify. The  
626 forcing temperature may contain many simultaneous sources of non-stationarity with different  
627 frequencies and magnitudes buried in the diel temperature records (e.g. caused by the local  
628 climate, seasonal shading, surface flow, etc.). Therefore, the detectability of transient flux  
629 magnitudes will depend on the strength of non-stationarity from other sources. In some cases it  
630 may become impossible to disentangle the diel frequency from other sources of non-stationarity.  
631 Our results illustrate that while signal processing is mandatory to extract harmonic amplitude  
632 and phases its limited ability to deal with signal non-stationarity thwarts the accurate delineation  
633 of transient fluxes and thermal diffusivities or sediment scour/deposition.

634 McCallum et al. [2012] observed that the thermal diffusivities calculated from heat tracing can  
635 temporarily exceed any physically plausible limits. Further, they warned that this could be due to  
636 violated boundary conditions for the analytical solution. Here, we show that the apparent  
637 “jumps” in thermal diffusivity originate from signal processing artifacts caused by transient  
638 water fluxes that impose sudden non-stationarity on the underlying temperature signal. These

639 signal features are too fast for methods that make use of Fourier based time-frequency  
640 transformation and are thus incorrectly delineated.

641 In a different study, Luce et al. [2013] proposed that streambed scouring could be inferred from  
642 quantifications of apparent variation in sensor spacing  $\Delta z$ , rather than thermal diffusivity.  
643 Tonina et al. [2014] tested the quantification of time-variant scour and deposition with analytical  
644 heat tracing in combination with DHR and Equations 9-11. While they tested the method's  
645 capability by manually changing the amount of sediment above the buried temperature sensor  
646 during times when the flux was relatively steady, naturally occurring sediment movement  
647 typically occurs when the stream discharge is high. This implies transient stream discharge  
648 conditions which are also the main driver for transient vertical fluxes. Gariglio et al. [2014]  
649 attributed highly variable thermal diffusivities with values exceeding physically plausible limits,  
650 as calculated during times of transient river discharge using DHR, to sediment scour/deposition.  
651 We point out that quantifying naturally occurring sediment movement, such as scour and  
652 depositional processes, using analytical heat tracing may be a challenging proposition. This is  
653 because a) the derivation for sensor spacing is the same but rearranged equation as that for  
654 thermal diffusivity (Equations 10 and 11) and results are prone to artifacts as illustrated earlier,  
655 and b) the natural example presented in Luce et al. [2013] suggests that the water flux was  
656 transient as indicated by the fluctuating river discharge data. Flux and diffusivity artifacts arising  
657 from signal non-stationarity, which are to be expected during transient discharge conditions  
658 when sediment movement likely occurs simultaneously, could thus easily be mistaken for  
659 scour/depositional processes. We demonstrate that heat tracing based on harmonic signals  
660 becomes increasingly unsuitable to quantify vertical fluxes, thermal diffusivities or sediment  
661 scour/deposition from temperature data under increasingly transient flow conditions.

662 Sediment temperature data reported in the literature and acquired during highly transient  
663 hydraulic events (e.g. floods) at the system boundary exhibit high non-stationarity in regards to  
664 harmonic components (e.g. see Barlow et al. [2009]; Mutiti and Levy [2010]). We expect that  
665 the risk of leakage due to signal time-frequency transformation, and associated impact on  
666 amplitude and phase data, will contribute considerable uncertainty to the delineation of transient  
667 fluxes, thermal diffusivities or sediment scour/deposition. Furthermore, flux transients often  
668 occur on time scales less than one harmonic cycle (e.g. duration of flood peak, dam releases or  
669 the onset or cessation of near-stream groundwater pumping). Consequently, to quantify highly  
670 transient fluxes and thermal diffusivity or sediment scour/deposition under such conditions we  
671 recommend that numerical approaches be deployed [e.g. Holzbecher, 2005; Voytek et al., 2013],



672 or that methods based on signal processing techniques offering improved delineation of transient  
673 processes from frequency-domain data are deployed or developed.

#### 674 4. Conclusion

675 A thorough analysis of Stallman's [1965] analytical solution reveals that changes in the vertical  
676 water flux induce non-stationarity in the temperature signal during its propagation. The severity  
677 of non-stationarity depends on the magnitude of the flux transient. A simulated worst case water  
678 velocity transient (step change from 0 to -1 m/d with harmonic amplitude of 3 °C) triggers an  
679 abrupt transition to non-stationarity in the sediment temperature signal. The response (difference  
680 between modeled temperature and analytical solution assuming steady-state velocity) depends  
681 on the thermal diffusivity and the onset of the velocity step change relative to the phase of the  
682 harmonic temperature boundary. The maximum response is ~2.3 °C and return to stationarity  
683 occurs within 1 harmonic cycle (= 1 day) for physically plausible sediment thermal diffusivities  
684 in the range of 0.02-0.13 m<sup>2</sup>/d.

685 Inverting transient vertical fluxes and thermal diffusivities from temperature records using  
686 analytical heat tracing relies either on the transformation of the signal from time to frequency  
687 domain, or extraction of time-variable amplitude and phase information of a fixed-frequency  
688 harmonic. Both are only possible with signal processing techniques. We benchmarked the ability  
689 of four commonly used signal processing methods (windowed Fourier transform (WFT),  
690 forward-backward zero phase filter (filtfilt), continuous wavelet transform (CWT) and dynamic  
691 harmonic regression (DHR)) to delineate signal non-stationarity implicit in the temperature-time  
692 signal. This was done by numerically simulating the transient advective thermal velocity with a  
693 harmonic temperature boundary and comparing the known to the inverted velocities obtained by  
694 the signal processing and the analytical solution. All the signal processing techniques were  
695 shown to offer poor time-domain resolution of frequency-domain features, and to erroneously  
696 spread amplitude and phase information across up to approx. 4 harmonic cycles (4 days). There  
697 is a technique and parameter dependent trade-off between magnitude and duration of the  
698 response to abrupt signal non-stationarity.

699 In essence, our analysis shows that the ability to accurately resolve flux transients with analytical  
700 heat tracing is currently limited by the signal processing, rather than the assumption of steady-  
701 state flow inherent to Stallman's [1965] analytical solution. This is because local signal  
702 stationarity is assumed for each extracted amplitude and/or phase value. The signal processing  
703 response appears to be independent of the advective thermal velocity step size, including  
704 reversal, for steps smaller than ±1 m/d. The match between modeled and inverted velocities  
705 improves with decreasing rates of velocity change. Implications on heat tracing are that: a) a  
706 sudden sharp transient in apparent velocity appears smoothed and earlier than the hydraulic

707 driver, and b) an apparent thermal diffusivity overshoot (undershoot) for a downward (upward)  
708 velocity change with values that can exceed physically plausible limits. The latter is caused by  
709 signal processing methods introducing phase artifacts originating from response to signal non-  
710 stationarity. While the thermal diffusivity anomaly can be used as an indication of a flux  
711 transient (including direction), the quantified flux and diffusivity values or sensor spacing  
712 (sediment scour/deposition) should not be trusted during that time.

713 Real-world temperature records contain non-stationarities caused by a range of different  
714 superimposed factors, such as abrupt hydrologic or meteoric changes, or anthropogenic  
715 disturbances. We applied the commonly used heat tracing techniques to numerically simulated  
716 streambed temperatures with the model driven by previously presented surface water  
717 temperature data [Rau et al., 2010] as the upper boundary. Inversion of fluxes and thermal  
718 diffusivities from the simulated temperatures reveals that, besides the erroneous temporal  
719 spreading of the flux transient (time-smearing), there are anomalies in the diffusivity results that  
720 originate from the signal processing techniques. The forward-backward zero-phase filter was  
721 identified as the best-performing amplitude and phase extraction method causing the least  
722 artifacts, but limited to producing 2 flux results per day.

723 Our results have significant implications for the practical application of inverting water fluxes,  
724 thermal diffusivities or sensor spacing (scour/deposition) from temperature data using  
725 increasingly popular methods that are based on harmonically forced analytical solutions. While  
726 these techniques are useful to estimate fluxes during times when hydraulic drivers indicate  
727 steady-state conditions, attention must be paid during transient conditions. This suggests that,  
728 when highly transient fluxes are to be calculated from temperature records, hydraulic heads  
729 should be monitored alongside temperature data, and that either numerical methods or new  
730 signal processing methods extracting features in the time domain must be applied. Besides the  
731 implications for heat tracing in near-surface water systems, our results point out that the  
732 response of signal processing techniques to non-stationary data must be carefully considered  
733 when time-varying physical processes are inferred from frequency-domain information in other  
734 geophysical datasets.

735 **Acknowledgements**

736 Funding was provided by the Gary Johnston fund that started the Chair of Water Management at  
737 UNSW Australia. Mark Cuthbert was supported by Marie Curie Research Fellowship funding  
738 from the European Community's Seventh Framework Programme [FP7/2007-2013] under grant  
739 agreement n.299091. Landon Halloran was supported by a UNSW School of Civil and  
740 Environmental Engineering scholarship and a Canadian "Fonds de Recherche du Québec -  
741 Nature et Technologies" (dossier: 173538). The data for this paper are available by contacting  
742 the corresponding author. We thank Giovanni Coco (editor) for handling our manuscript and  
743 Jason Kean (associate editor) for very comprehensive and helpful feedback. Further, we are  
744 grateful to Jim Constantz and 2 anonymous reviewers for their constructive suggestions that  
745 have significantly strengthened this work.

746 **References**

- 747 Anderson, M. P. (2005), Heat as a Ground Water Tracer, *Ground Water*, 43(6), 951-968, doi:  
748 10.1111/j.1745-6584.2005.00052.x.
- 749 Barlow, J. R. B., and R. H. Coupe (2009), Use of heat to estimate streambed fluxes during  
750 extreme hydrologic events, *Water Resources Research*, 45, W01403, doi:  
751 10.1029/2007WR006121.
- 752 Best, A. I., C. McCann, and J. Sothcott (1994), The relationships between the velocities,  
753 attenuations and petrophysical properties of reservoir sedimentary rocks1, *Geophysical*  
754 *Prospecting*, 42(2), 151-178, doi: 10.1111/j.1365-2478.1994.tb00204.x.
- 755 Constantz, J. (2008), Heat as a tracer to determine streambed water exchanges, *Water Resources*  
756 *Research*, 44, -, doi: 10.1029/2008WR006996.
- 757 COMSOL (2014), COMSOL Multiphysics Version 5, COMSOL Inc., Burlington, MA, USA.
- 758 Cuthbert, M. O. (2010), An improved time series approach for estimating groundwater recharge  
759 from groundwater level fluctuations, *Water Resources Research*, 46(9), W09515, doi:  
760 10.1029/2009WR008572.
- 761 Cuthbert, M. O., and R. Mackay (2013), Impacts of nonuniform flow on estimates of vertical  
762 streambed flux, *Water Resources Research*, 49(1), 19-28, doi: 10.1029/2011WR011587.
- 763 Cuthbert, M. O., R. Mackay, V. Durand, M.-F. Aller, R. B. Greswell, and M. O. Rivett (2010),  
764 Impacts of river bed gas on the hydraulic and thermal dynamics of the hyporheic zone, *Advances*  
765 *in Water Resources*, 33, 1347-1358, doi: 10.1016/j.advwatres.2010.09.014.

766 Erickson, J. (2014), Continuous wavelet transform and inverse, Matlab Central,  
767 <[http://www.mathworks.com/matlabcentral/fileexchange/20821-continuous-wavelet-transform-](http://www.mathworks.com/matlabcentral/fileexchange/20821-continuous-wavelet-transform-and-inverse)  
768 [and-inverse](http://www.mathworks.com/matlabcentral/fileexchange/20821-continuous-wavelet-transform-and-inverse)>, updated: 14/10/2014, accessed: Jan 2015.

769 Fanelli, R. M., and L. K. Lautz (2008), Patterns of water, heat, and solute flux through  
770 streambeds around small dams., *Ground Water*, 46, 671-687, doi: 10.1111/j.1745-  
771 6584.2008.00461.x.

772 Gordon, R. P., L. K. Lautz, M. A. Briggs, and J. M. McKenzie (2012), Automated calculation of  
773 vertical pore-water flux from field temperature time series using the VFLUX method and  
774 computer program, *Journal of Hydrology*, 420-421, 142-158, doi:  
775 10.1016/j.jhydrol.2011.11.053.

776 Goto, S., M. Yamano, and M. Kinoshita (2005), Thermal response of sediment with vertical  
777 fluid flow to periodic temperature variation at the surface, *J Geophys Res-Sol Ea*, 110, B01106,  
778 doi: 10.1029/2004JB003419.

779 Gariglio, F. P., D. Tonina, and C. H. Luce (2013), Spatiotemporal variability of hyporheic  
780 exchange through a pool-riffle-pool sequence, *Water Resources Research*, 49(11), 7185-7204,  
781 doi: 10.1002/wrcr.20419.

782 Harris, F. J. (1978), On the use of windows for harmonic analysis with the discrete Fourier  
783 transform, *Proceedings of the IEEE*, 66(1), 51-83, doi: 10.1109/PROC.1978.10837.

784 Hatch, C. E., A. T. Fisher, J. S. Revenaugh, J. Constantz, and C. Ruehl (2006), Quantifying  
785 surface water-groundwater interactions using time series analysis of streambed thermal records:  
786 Method development, *Water Resources Research*, 42, W10410, doi: 10.1029/2005WR004787.

787 Havin, V., and B. Jöricke (1994), *The uncertainty principle in harmonic analysis*, Springer.

788 Holzbecher, E. (2005), Inversion of temperature time series from near-surface porous sediments,  
789 *Journal of Geophysics and Engineering*, 2, 343-348, doi: 10.1088/1742-2132/2/4/S07.

790 Irvine, D. J., R. H. Cranswick, C. T. Simmons, M. A. Shanafield, and L. K. Lautz (2015), The  
791 effect of streambed heterogeneity on groundwater-surface water exchange fluxes inferred from  
792 temperature time series, *Water Resources Research*, n/a-n/a, doi: 10.1002/2014WR015769.

793 Jensen, J. K., and P. Engesgaard (2011), Nonuniform Groundwater Discharge across a  
794 Streambed: Heat as a Tracer, *Vadose Zone J*, 10, 98, doi: 10.2136/vzj2010.0005.

795 Keery, J. S., and A. Binley (2007), Temperature measurements for determining groundwater–  
796 surface water fluxes, *Rep. Science Report SC030155/SR9*, Environment Agency & Lancaster  
797 University, Bristol, UK.

798 Keery, J., A. Binley, N. Crook, and J. W. N. Smith (2007), Temporal and spatial variability of  
799 groundwater–surface water fluxes: Development and application of an analytical method using  
800 temperature time series, *Journal of Hydrology*, 336, 1-16, doi: 10.1016/j.jhydrol.2006.12.003.

801 Lautz, L. K. (2010), Impacts of nonideal field conditions on vertical water velocity estimates  
802 from streambed temperature time series, *Water Resources Research*, 46, W01509, doi:  
803 10.1029/2009WR007917.

804 Lautz, L. K. (2012), Observing temporal patterns of vertical flux through streambed sediments  
805 using time-series analysis of temperature records, *Journal of Hydrology*, 464–465, 199–215, doi:  
806 10.1016/j.jhydrol.2012.07.006.

807 Luce, C. H., D. Tonina, F. Gariglio, and R. Applebee (2013), Solutions for the diurnally forced  
808 advection-diffusion equation to estimate bulk fluid velocity and diffusivity in streambeds from  
809 temperature time series, *Water Resources Research*, 49(1), 488-506, doi:  
810 10.1029/2012WR012380.

811 McCallum, A. M., M. S. Andersen, G. C. Rau, and R. I. Acworth (2012), A 1D analytical  
812 method for estimating surface water groundwater interactions and effective thermal diffusivity  
813 using temperature time series, *Water Resources Research*, 48, W11532.

814 McCallum, A. M., M. S. Andersen, G. C. Rau, J. R. Larsen, and R. I. Acworth (2014), River-  
815 aquifer interactions in a semiarid environment investigated using point and reach measurements,  
816 *Water Resources Research*, 50(4), 2815-2829, doi: 10.1002/2012WR012922.

817 Munz, M., S. E. Oswald, and C. Schmidt (2011), Sand box experiments to evaluate the influence  
818 of subsurface temperature probe design on temperature based water flux calculation, *Hydrology  
819 and Earth System Sciences Discussions*, 8, 6155-6197, doi: 10.5194/hessd-8-6155-2011.

820 Mutiti, S., and J. Levy (2010), Using temperature modeling to investigate the temporal  
821 variability of riverbed hydraulic conductivity during storm events, *Journal of Hydrology*, 388,  
822 321-334, doi: 10.1016/j.jhydrol.2010.05.011.

823 Onderka, M., S. Banzhaf, T. Scheytt, and A. Krein (2013), Seepage velocities derived from  
824 thermal records using wavelet analysis, *Journal of Hydrology*, 479(0), 64-74, doi:  
825 10.1016/j.jhydrol.2012.11.022.

826 Oppenheim, A. V., R. W. Schafer, and J. R. Buck (1989), *Discrete-time signal processing*,  
827 Prentice-hall Englewood Cliffs.

828 Pidlisecky, A., and R. Knight (2011), The Use of Wavelet Analysis to Derive Infiltration Rates  
829 from Time-Lapse One-Dimensional Resistivity Records, *Vadose Zone*, 10(2), 697-705, doi:  
830 10.2136/vzj2010.0049.

831 Rau, G. C., M. S. Andersen, and R. I. Acworth (2012a), Experimental investigation of the  
832 thermal dispersivity term and its significance in the heat transport equation for flow in  
833 sediments, *Water Resources Research*, 48, W03511, doi: 10.1029/2011WR011038.

834 Rau, G. C., M. S. Andersen, and R. I. Acworth (2012b), Experimental investigation of the  
835 thermal time-series method for surface water-groundwater interactions, *Water Resources*  
836 *Research*, 48, W03530, doi: 10.1029/2011WR011560.

837 Rau, G. C., M. S. Andersen, A. M. McCallum, and R. I. Acworth (2010), Analytical methods  
838 that use natural heat as a tracer to quantify surface water-groundwater exchange, evaluated using  
839 field temperature records, *Hydrogeol J*, 18, 1093-1110, doi: 10.1007/s10040-010-0586-0.

840 Roshan, H., G. C. Rau, M. S. Andersen, and I. R. Acworth (2012), Use of heat as tracer to  
841 quantify vertical streambed flow in a two-dimensional flow field, *Water Resources Research*,  
842 48(10), W10508, doi: 10.1029/2012WR011918.

843 Shanafield, M., C. Hatch, and G. Pohl (2011), Uncertainty in thermal time series analysis  
844 estimates of streambed water flux, *Water Resources Research*, 47, W03504, doi:  
845 10.1029/2010WR009574.

846 Soto-López, C. D., T. Meixner, and T. P. A. Ferré (2011), Effects of measurement resolution on  
847 the analysis of temperature time series for stream-aquifer flux estimation, *Water Resources*  
848 *Research*, 47, W12602, doi: 10.1029/2011WR010834.

849 Stallman, R. W. (1965), Steady One-Dimensional Fluid Flow in a Semi-Infinite Porous Medium  
850 with Sinusoidal Surface Temperature, *J Geophys Res*, 70, 2821-2827, doi:  
851 10.1029/JZ070i012p02821.

852 Suzuki, S. (1960), Percolation Measurements Based on Heat Flow Through Soil with Special  
853 Reference to Paddy Fields, *J Geophys Res*, 65, 2883, doi: 10.1029/JZ065i009p02883.

854 Swanson, T. E., and M. B. Cardenas (2010), Diel heat transport within the hyporheic zone of a  
855 pool-riffle-pool sequence of a losing stream and evaluation of models for fluid flux estimation  
856 using heat, *Limnol. Oceanogr.*, 55, 1741-1754, doi: 10.4319/lo.2010.55.4.1741.

857 Swanson, T. E., and M. B. Cardenas (2011), Ex-Stream: A MATLAB program for calculating  
858 fluid flux through sediment–water interfaces based on steady and transient temperature profiles,  
859 *Computers & Geosciences*, 37, 1664-1669, doi: 10.1016/j.cageo.2010.12.001.

860 Tonina, D., C. Luce, and F. Gariglio (2014), Quantifying streambed deposition and scour from  
861 stream and hyporheic water temperature time series, *Water Resources Research*, 50(1), 287-292,  
862 doi: 10.1002/2013WR014567.

863 Torrence, C., and G. P. Compo (1998), A practical guide to wavelet analysis, *Bulletin of the*  
864 *American Meteorological society*, 79(1), 61-78.

865 Vogt, T., P. Schneider, L. Hahn-Woernle, and O. A. Cirpka (2010), Estimation of seepage rates  
866 in a losing stream by means of fiber-optic high-resolution vertical temperature profiling, *Journal*  
867 *of Hydrology*, 380, 154-164, doi: 10.1016/j.jhydrol.2009.10.033.

868 Voytek, E. B., A. Drenkelfuss, F. D. Day-Lewis, R. Healy, J. W. Lane, and D. Werkema (2013),  
869 1DTempPro: Analyzing Temperature Profiles for Groundwater/Surface-water Exchange,  
870 *Groundwater*, doi: 10.1111/gwat.12051.

871 Wörman, A., J. Riml, N. Schmadel, B. T. Neilson, A. Bottacin-Busolin, and J. E. Heavilin  
872 (2012), Spectral scaling of heat fluxes in streambed sediments, *Geophysical Research Letters*,  
873 39(23), L23402, doi: 10.1029/2012GL053922.

874 Wu, W., M. A. Geller, and R. E. Dickinson (2002), A case study for land model evaluation:  
875 Simulation of soil moisture amplitude damping and phase shift, *Journal of Geophysical*  
876 *Research: Atmospheres*, 107(D24), 4793, doi: 10.1029/2001JD001405.

877 Young, P. C., D. J. Pedregal, and W. Tych (1999), Dynamic harmonic regression, *Journal of*  
878 *Forecasting*, 18, 369-394, doi: 10.1002/(SICI)1099-131X(199911)18:6<369::AID-  
879 FOR748>3.0.CO;2-K.



880 **Figure captions**

881 Figure 1: Damping of amplitude (a) and shifting of phase (b) with depth for a sinusoid with  
882 frequency of 1 cpd calculated using Stallman's [1965] analytical solution. Shaded areas  
883 represent ranges based on effective thermal diffusivities  $D_{\min} = 0.02 \text{ m}^2/\text{d}$ ,  $D_{\text{avg}} = 0.075 \text{ m}^2/\text{d}$   
884 and  $D_{\max} = 0.13 \text{ m}^2/\text{d}$  as reported in the literature [Shanafield et al., 2011; McCallum et al.,  
885 2012]. Dashed horizontal lines show the depths at which temperature time-series were output  
886 from the numerical model.

887 Figure 2: a) An example of multi-level temperature harmonics in response to a step change in  
888 vertical water velocity as output from the numerical model. Here,  $\Delta z$  refers to sensor spacing of  
889 0, 0.05, 0.2 and 0.4 m from the top of the sediment plotted with increasing intensity of black  
890 color. The data serves to illustrate that a stationary harmonic is transformed into a non-stationary  
891 harmonic through a transient in the vertical water velocity. b) Modeled multi-level temperature  
892 data using real sediment temperature measurements at the streambed surface (from Rau et al.  
893 [2010]) as a boundary for the same velocity as in a).

894 Figure 3: a) The thermal response to a transient water velocity: The temperature difference  
895 between numerically modeled and analytically calculated harmonics due to a step change in  
896 velocity from 0 to -1 m/d for  $D_{\min} = 0.02 \text{ m}^2/\text{d}$ ,  $D_{\text{avg}} = 0.075 \text{ m}^2/\text{d}$  and  $D_{\max} = 0.13 \text{ m}^2/\text{d}$  at  
897 sensor spacing of  $\Delta z = 0.1$  and  $\Delta z = 0.2$  m. b) Same as a) but for the step change occurring at 8  
898 different times (separated by 0.125 d or  $\pi/4$ ) relative to the start of the harmonic temperature  
899 signal used as boundary condition at  $z = 0$  m (shown on right axis, with  $D_{\text{avg}} = 0.075 \text{ m}^2/\text{d}$  and  
900 sensor spacing  $\Delta z = 0.2$  m.

901 Figure 4: Amplitude and phase response of common signal extraction methods (rows from top to  
902 bottom: WFT, filtfilt, CWT and DHR) to the non-stationarity introduced by a step velocity  
903 increase. Line color becomes lighter with increasing depth. Left column contains amplitudes,  
904 right column contains phases. Note that the values obtained from filtfilt (c and d) are plotted  
905 with dots whereas the lines are shown for visual improvement.

906 Figure 5: Vertical advective thermal velocities (left column: a, c, e, g) and thermal diffusivities  
907 (right column: b, d, f, h) inverted using amplitudes and phases from peak picking applied to raw  
908 data (red markers) as well as after applying 4 different signal processing methods (blue markers)  
909 to the model temperature output. The different cases are in rows from top to bottom: 0 to -1 m/d

910 (a-b), 0 to 1 m/d (c-d), -1 m/d to 1 m/d (e-f), 1 m/d to -1 m/d (g-h). Refer to Figures 6 and 7 for  
911 different velocity steps.

912 Figure 6: Downward advective thermal velocities (left column: a, c, e, g) and thermal  
913 diffusivities (right column: b, d, f, h) inverted using amplitudes and phases from peak picking  
914 applied to raw data (red markers) as well as after applying 4 different signal processing methods  
915 (blue markers) to the model temperature output. The different cases are in rows from top to  
916 bottom: 0 to -0.01 m/d (a-b), 0 to -0.1 m/d (c-d), 0 m/d to -0.5 m/d (e-f), 0 m/d to -5 m/d (g-h).

917 Figure 7: Upward advective thermal velocities (left column: a, c, e) and thermal diffusivities  
918 (right column: b, d, f) inverted using amplitudes and phases from peak picking applied to raw  
919 data (red markers) as well as after applying 4 different signal processing methods (blue markers)  
920 to the model temperature output. The different cases are in rows from top to bottom: 0 to 0.1 m/d  
921 (a-b), 0 to 0.5 m/d (c-d), 0 m/d to 2 m/d (e-f).

922 Figure 8: Vertical advective thermal velocities (left column: a, c, e, g) and thermal diffusivities  
923 (right column: b, d, f, h) inverted using amplitudes and phases from peak picking applied to raw  
924 data (red markers) as well as after applying 4 different signal processing methods (blue markers)  
925 to the model temperature output. The different scenarios are a linear change of advective thermal  
926 velocity from 0 to -1 m/d over a total time period of (in rows from top to bottom): 0.5 days (a-b),  
927 1 day (c-d), 2 days (e-f) and 4 days (g-h).

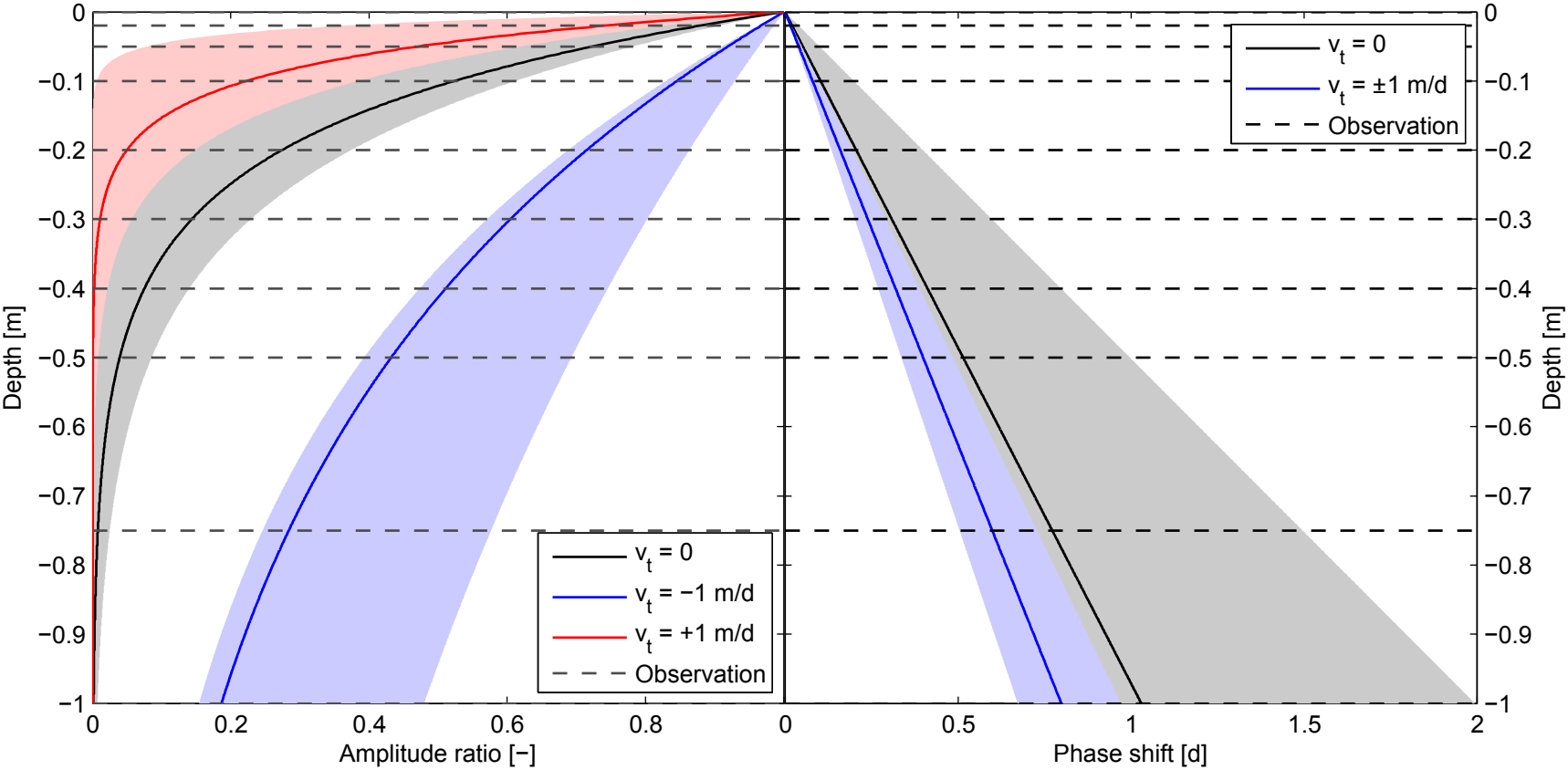
928 Figure 9: a) Temperature output obtained from the numerical model at different depths (0, 0.05,  
929 0.2 and 0.4 m from the top of the sediment) using measured surface water temperature data as  
930 the top boundary (from Rau et al. [2010]). b) Advective thermal velocities and c) thermal  
931 diffusivities inverted after the data has been processed with 4 different amplitude and phase  
932 extraction methods.

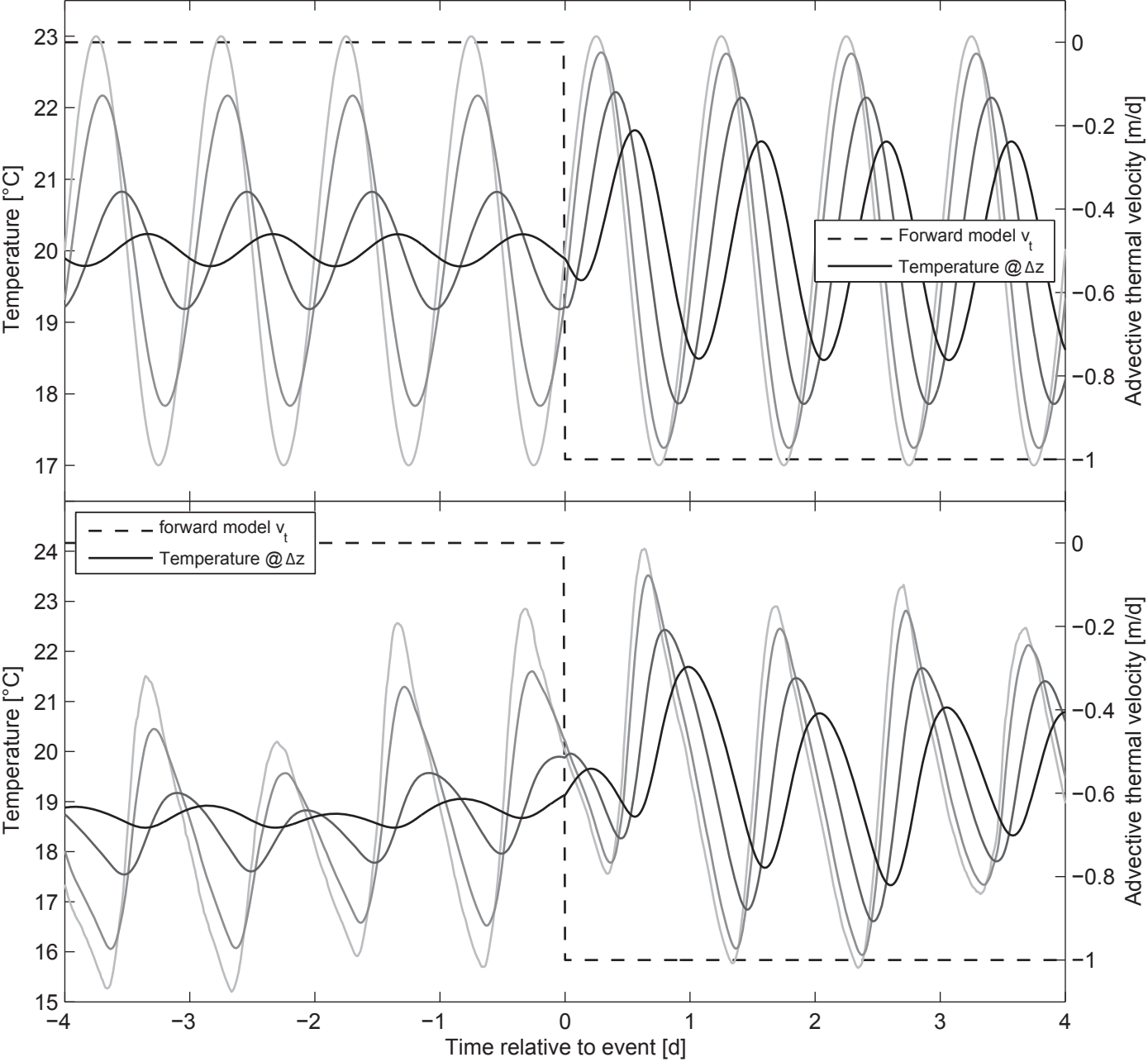
933

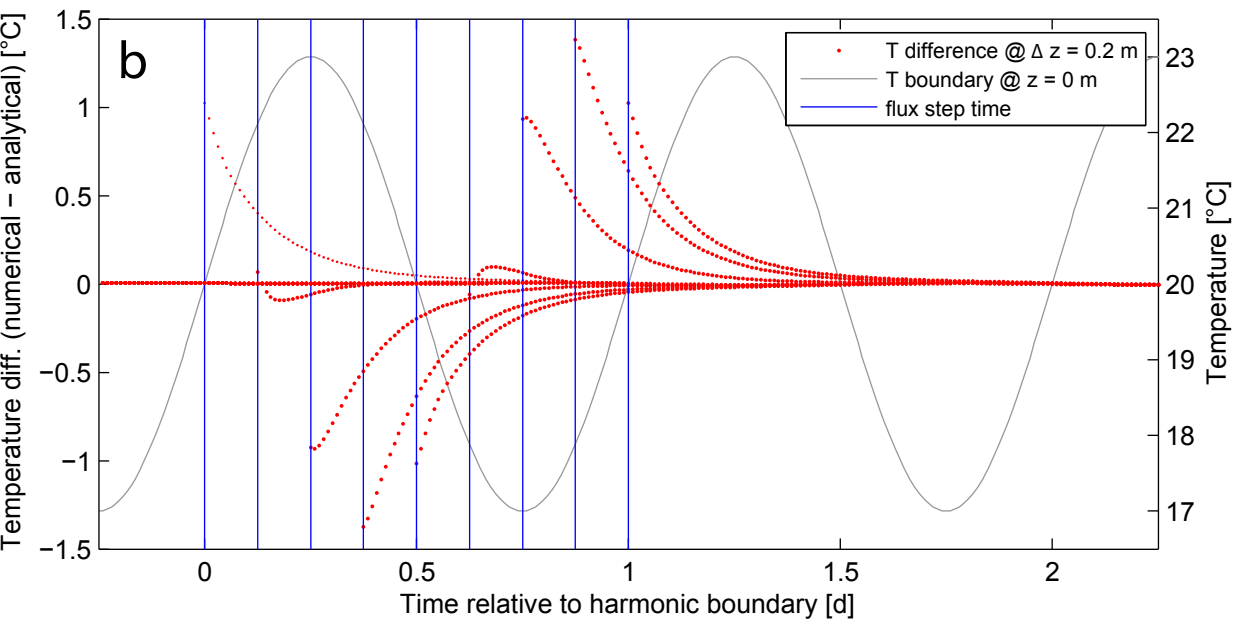
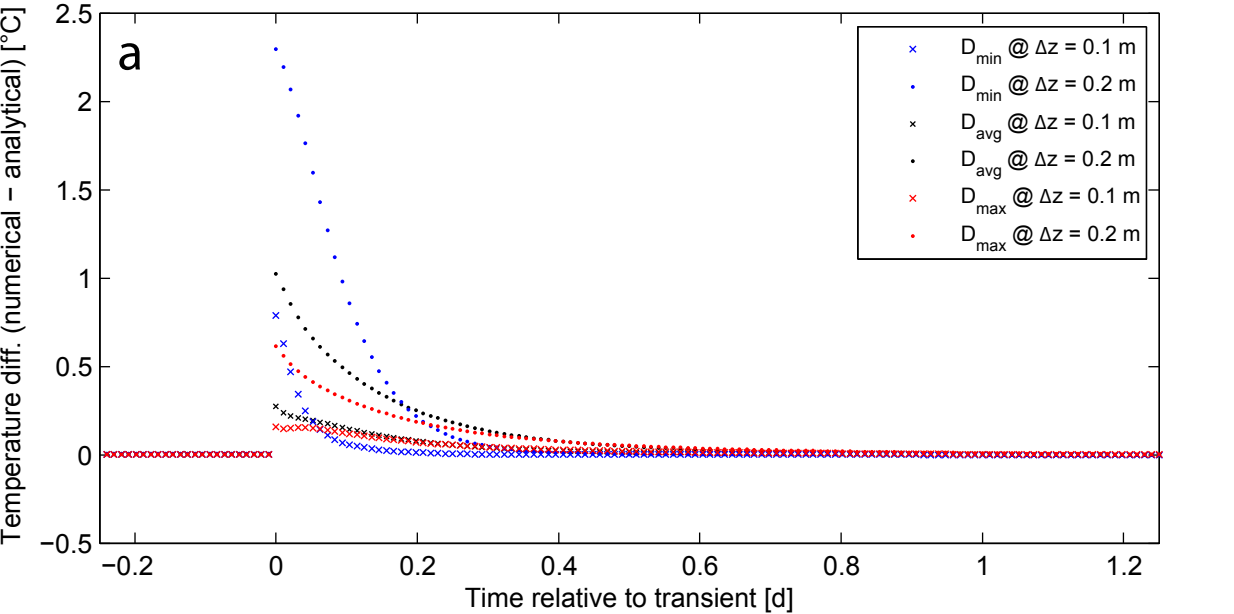
934 **Table captions**

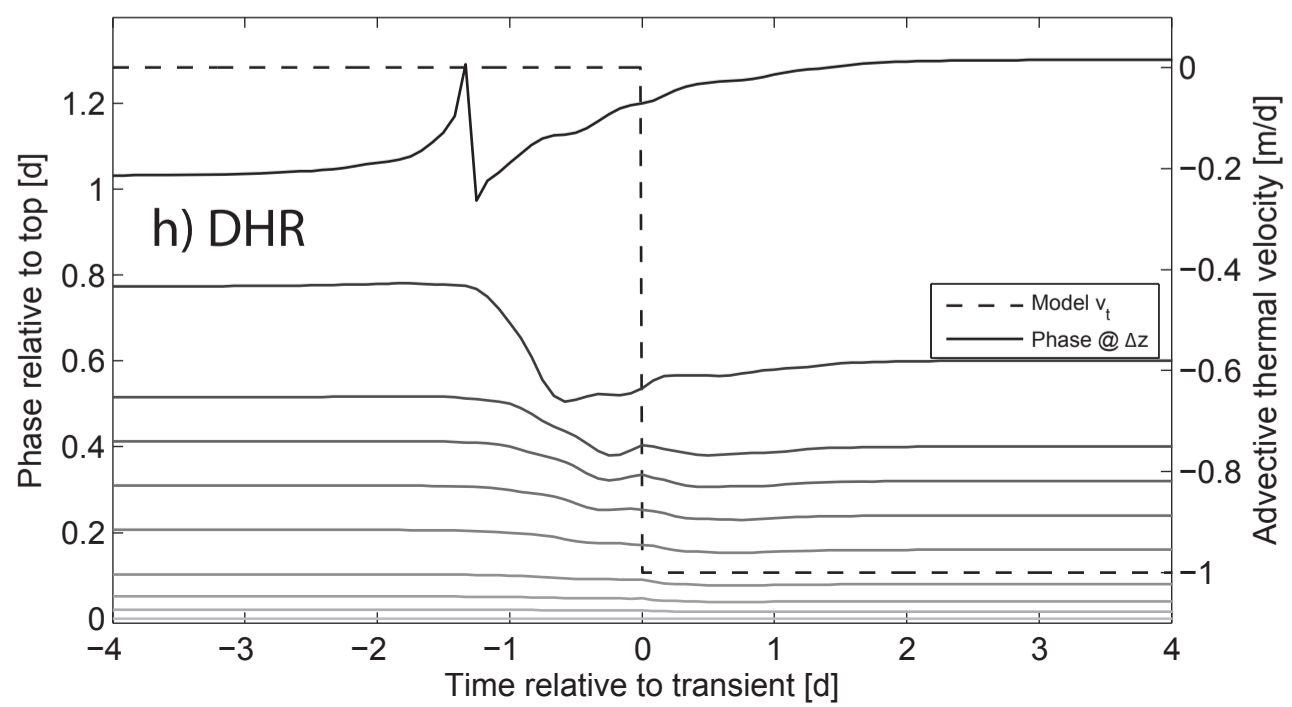
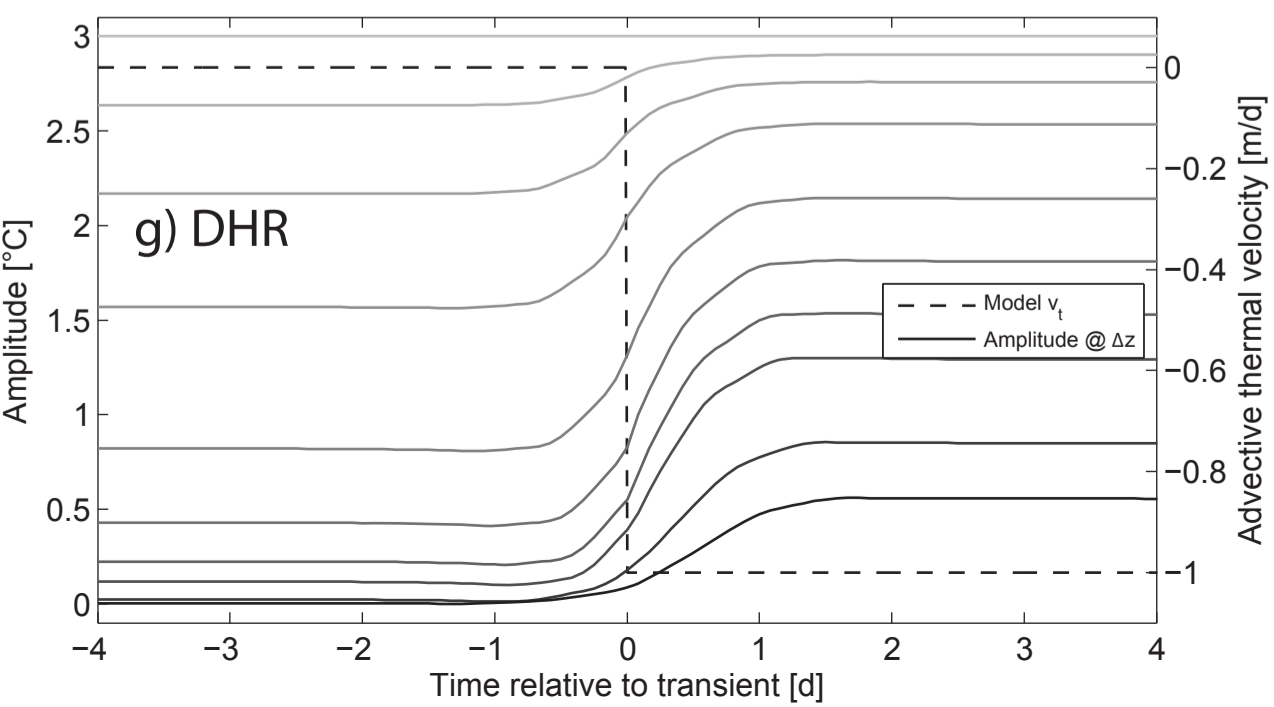
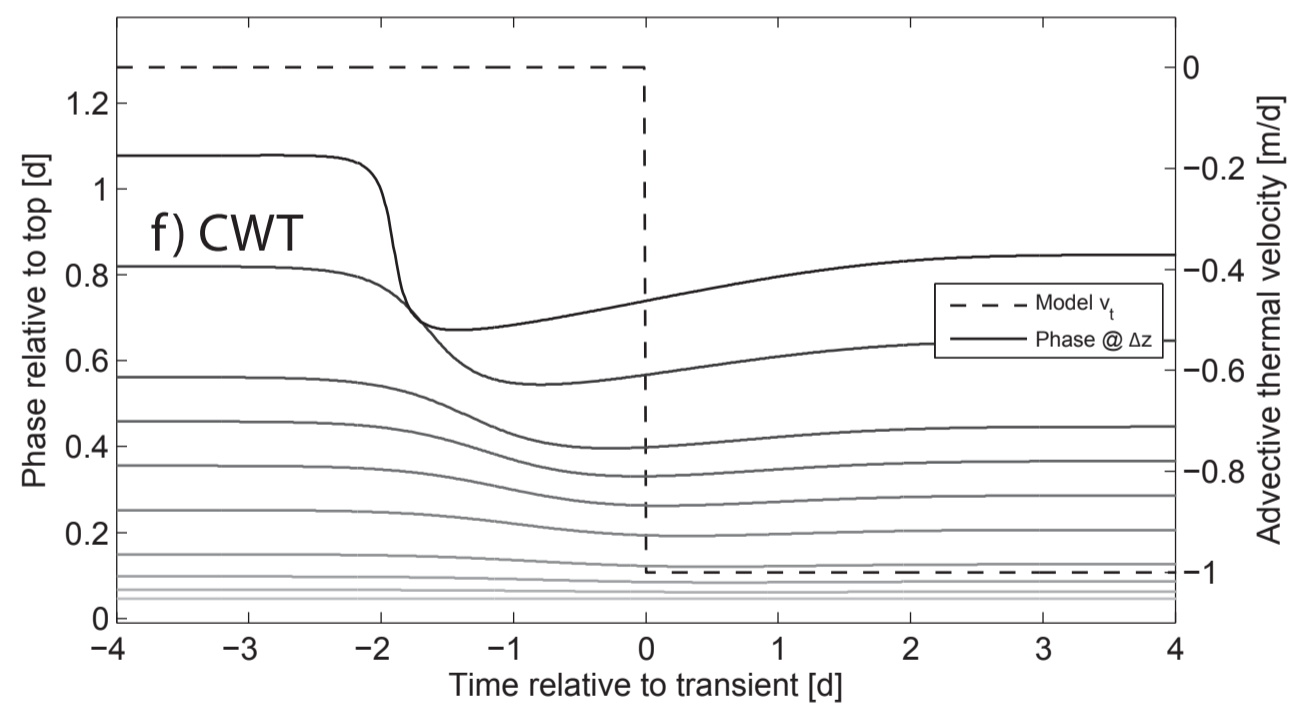
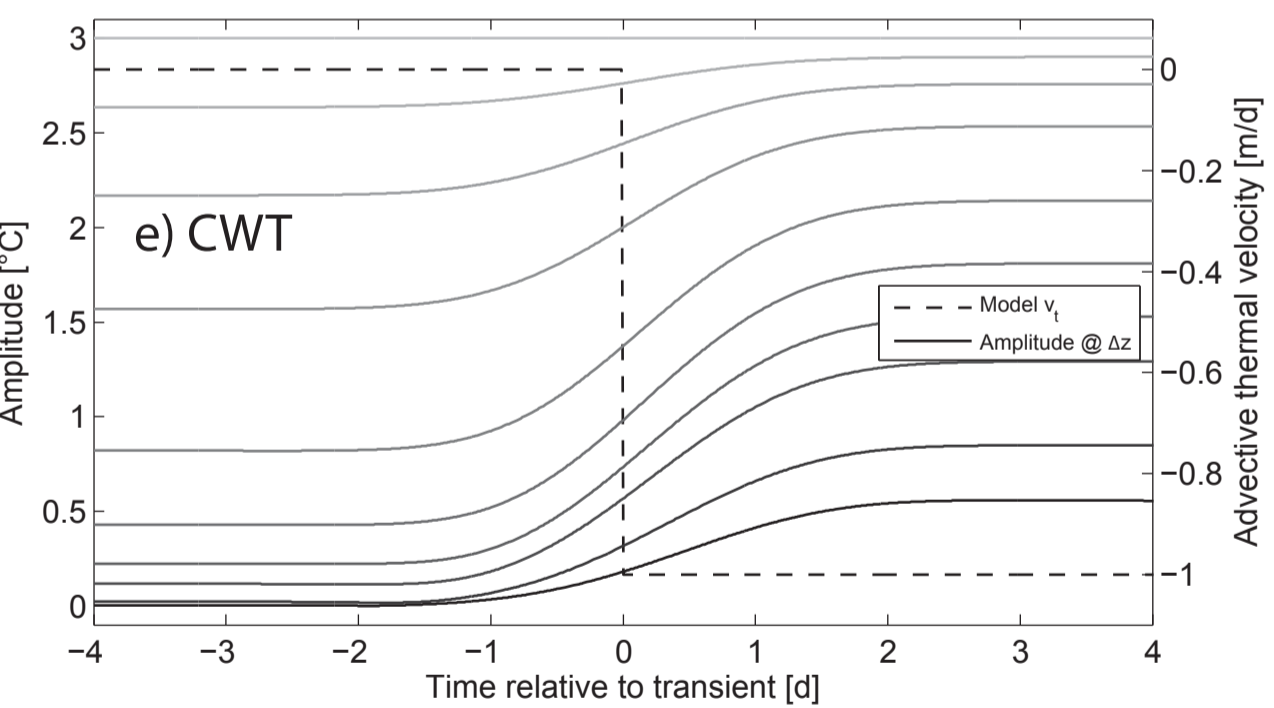
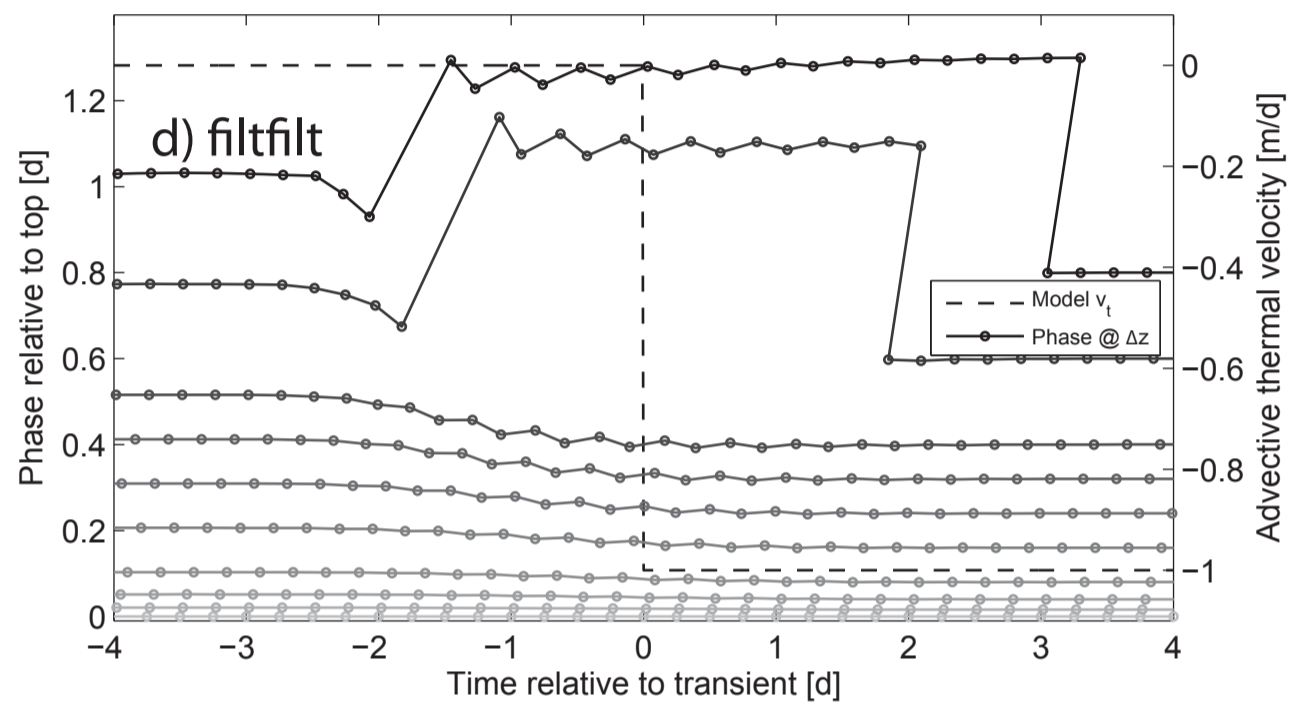
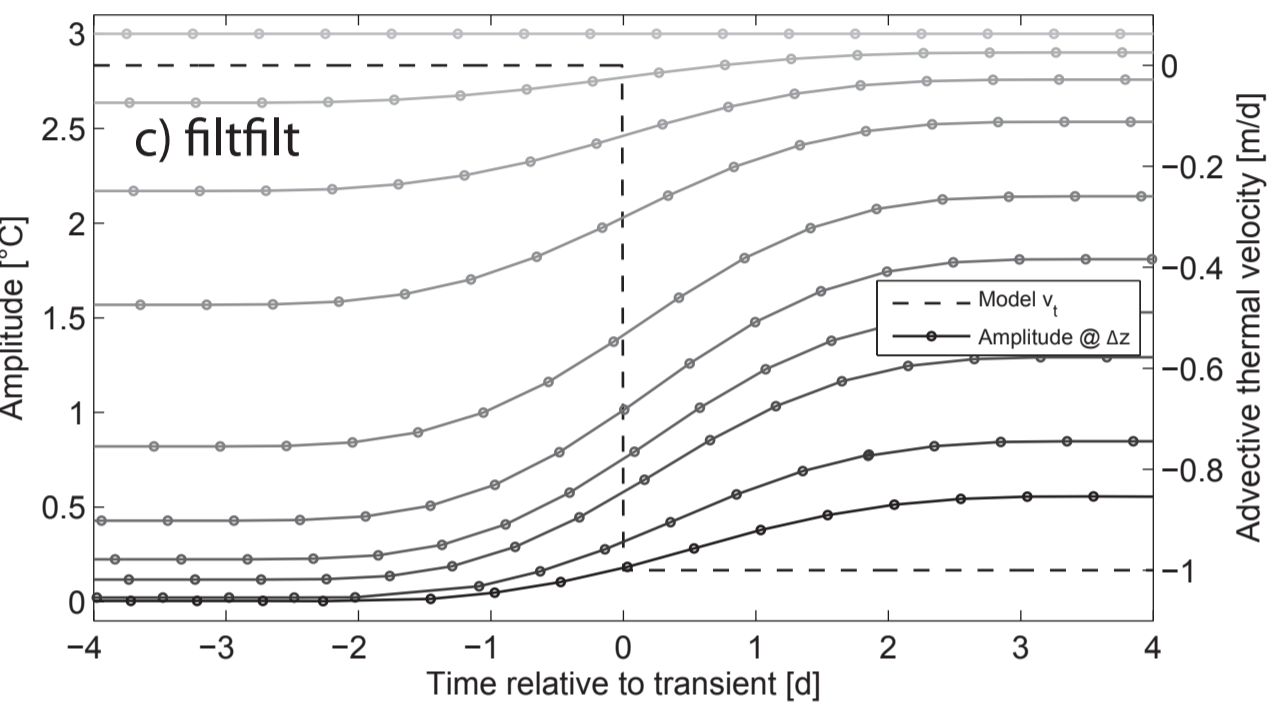
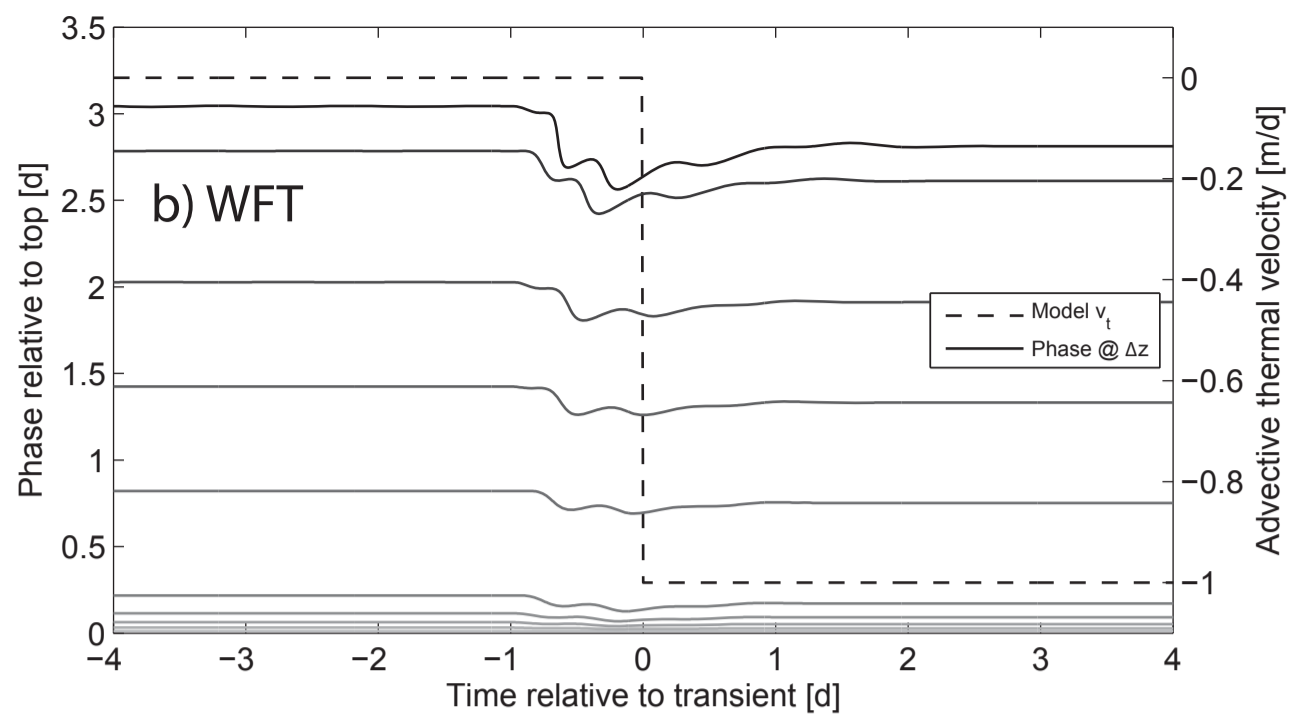
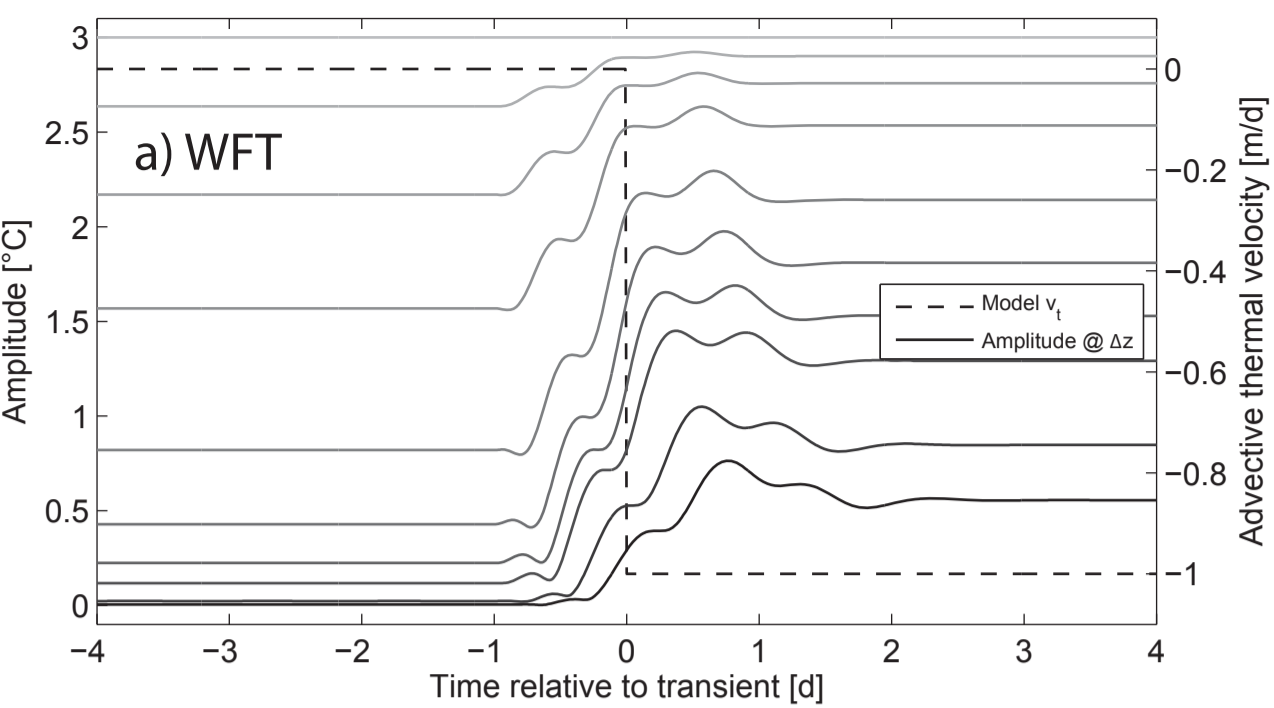
935 Table 1: Summary of maximum error and root mean square error (RMSE) calculated from  
936 modeled and inverted advective thermal velocities using unfiltered and filtered temperature data  
937 for the same magnitude velocity transients (0 to -1 m/d) but for different rates of velocity  
938 change. The values in this table represent a quantification of the results in Figure 8a, 8c, 8e, 8g  
939 and Figure 5a.

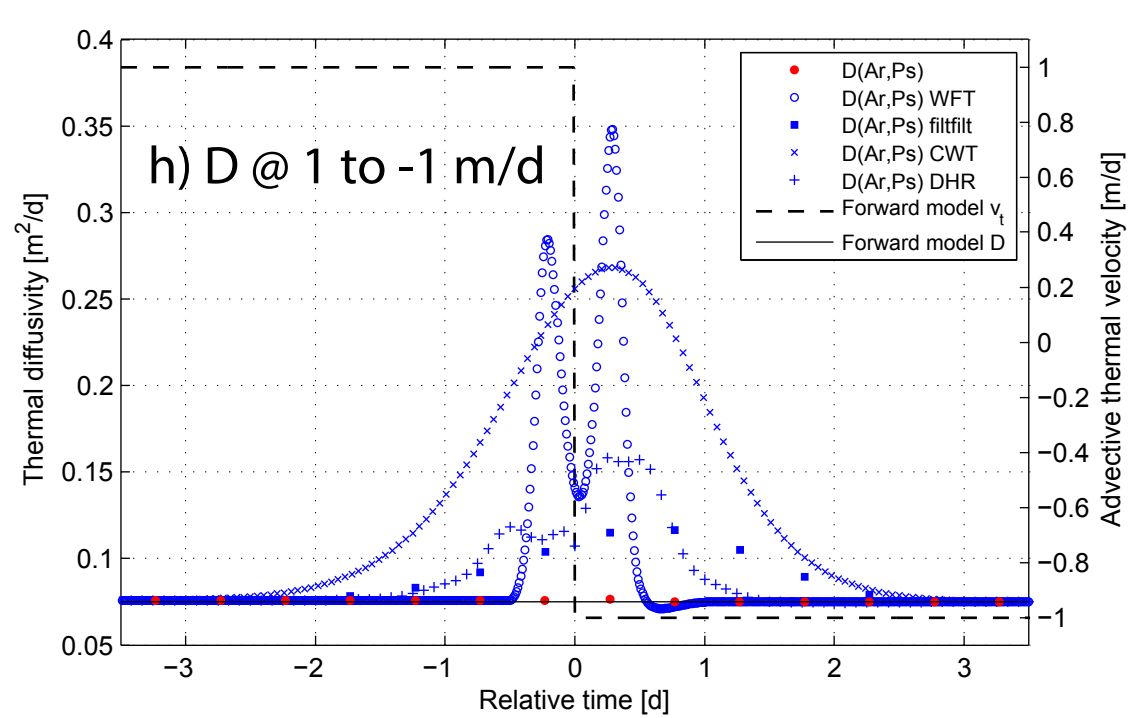
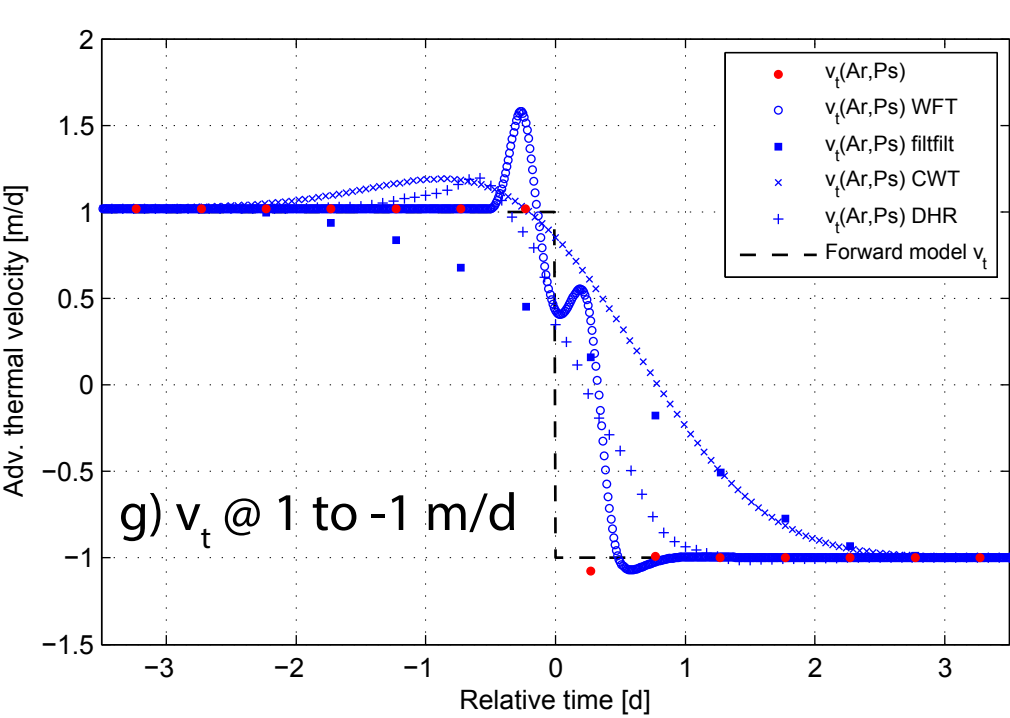
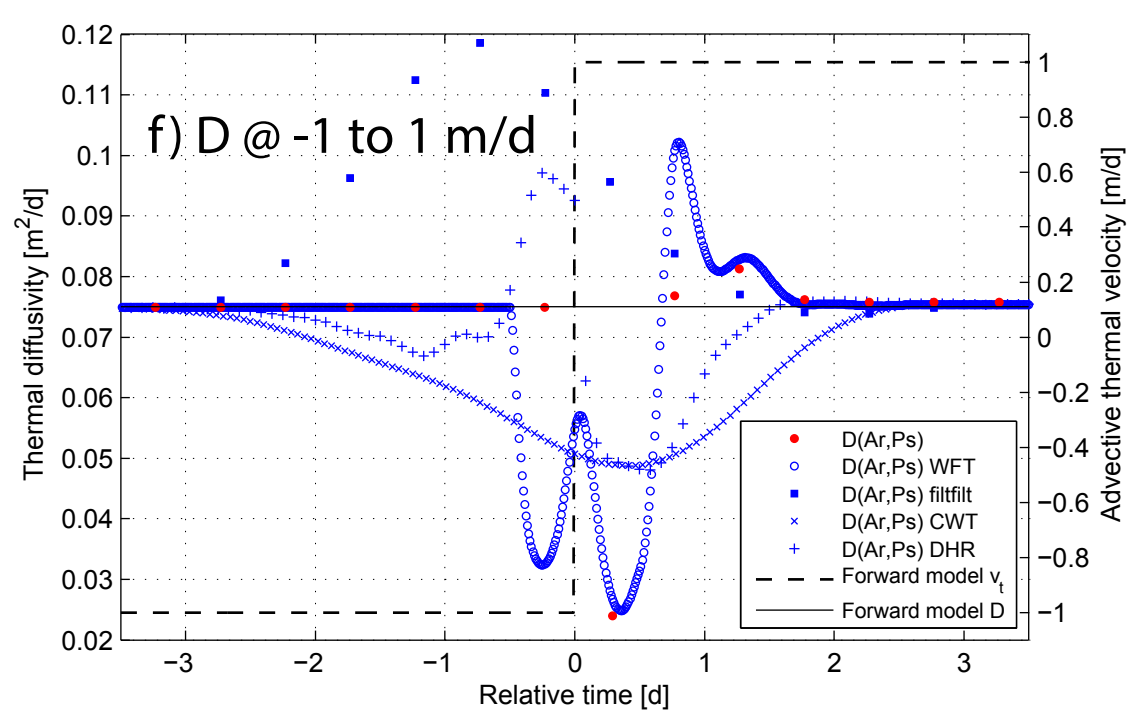
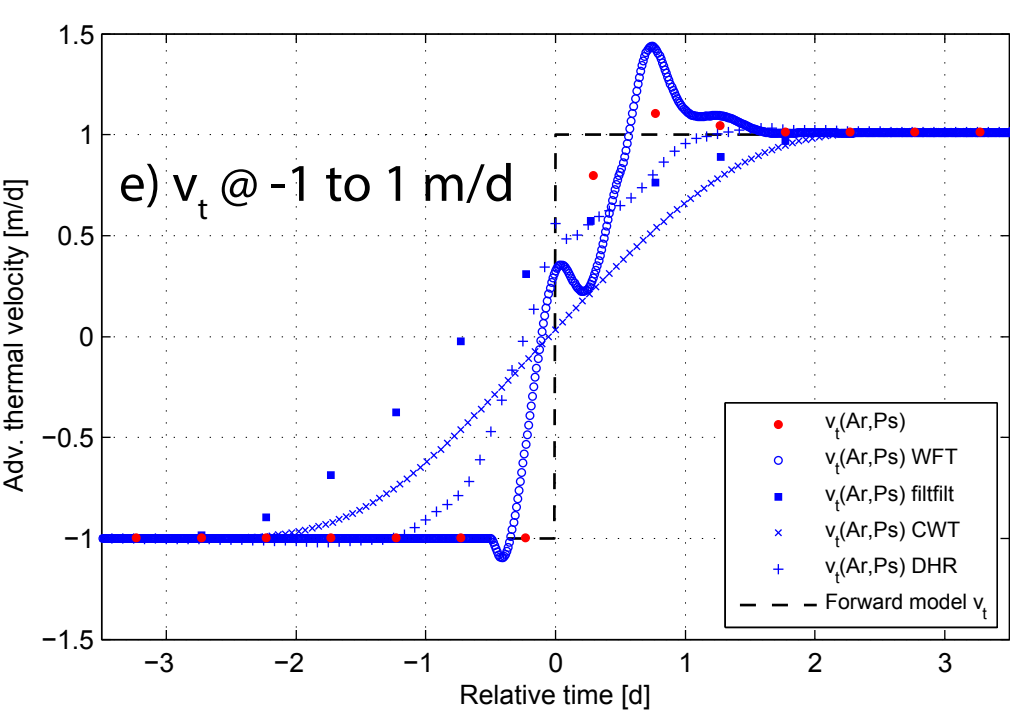
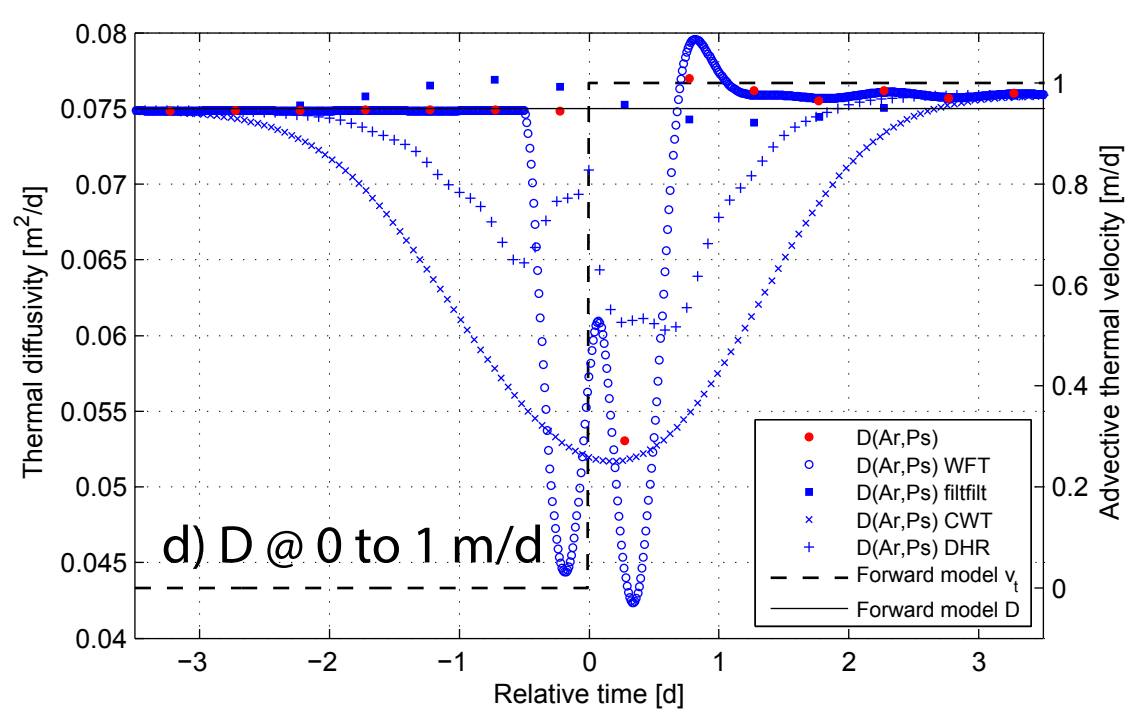
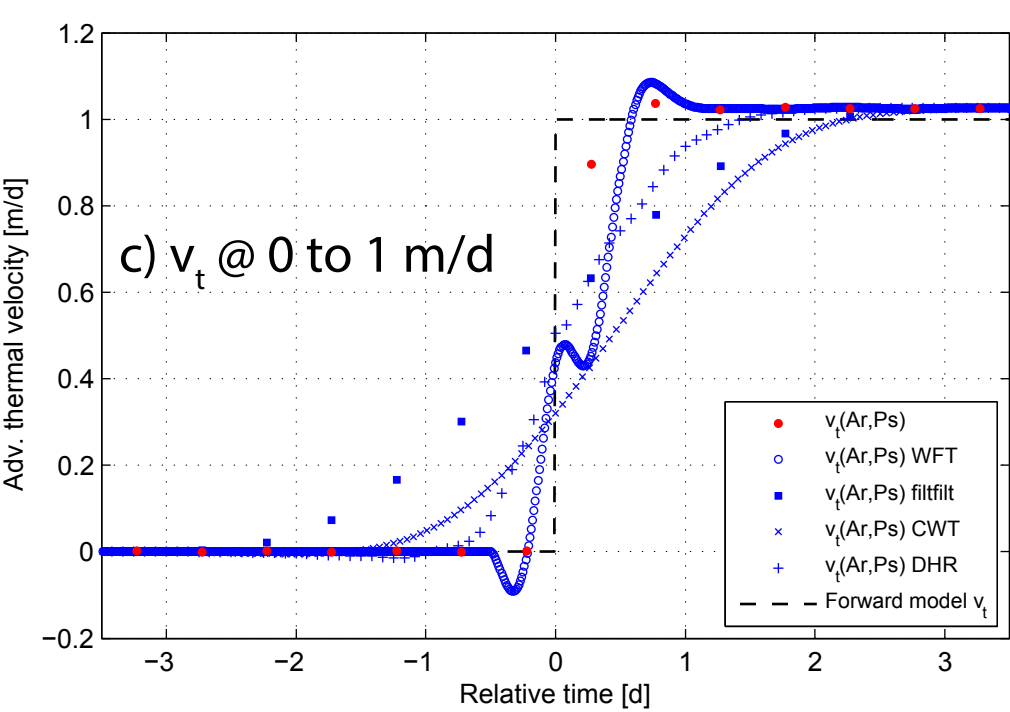
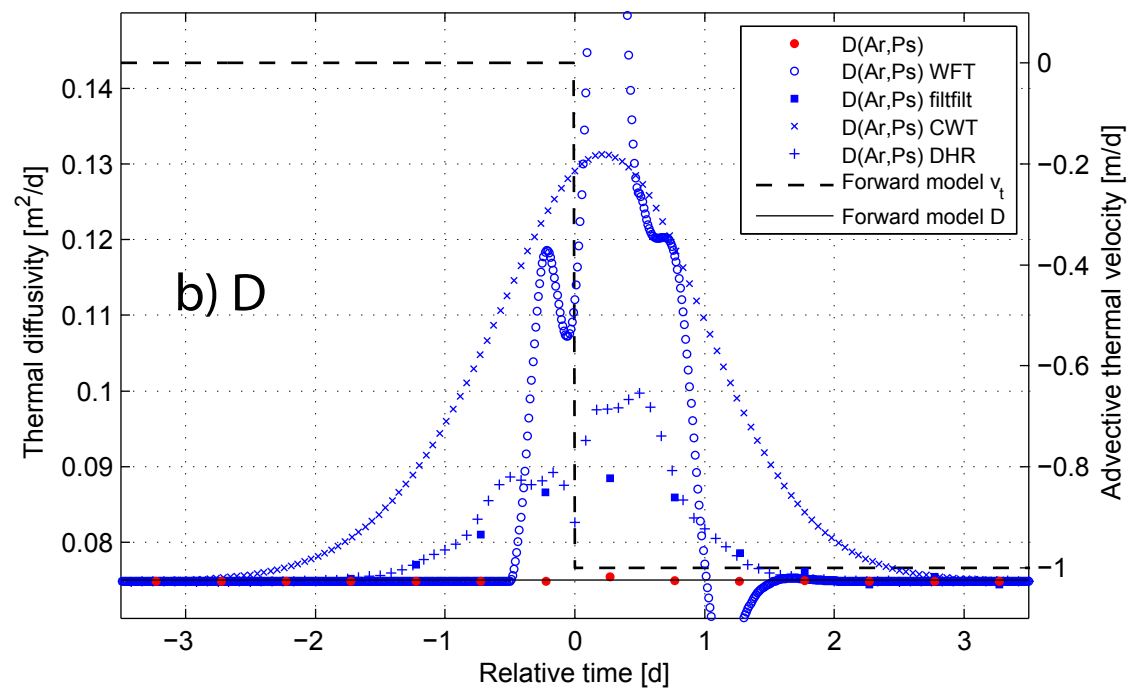
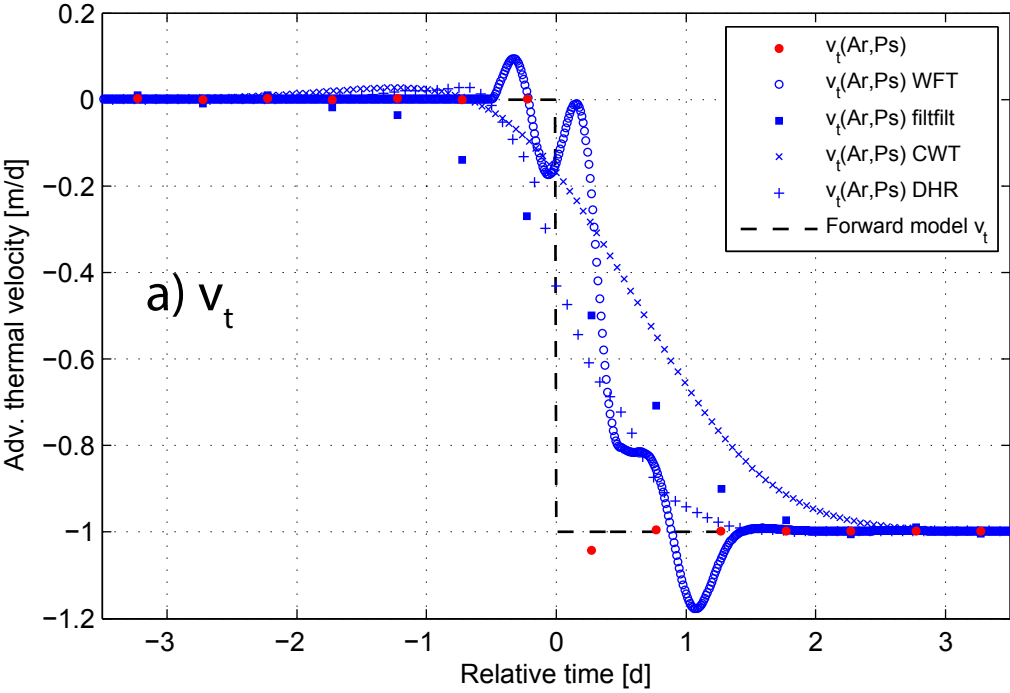
940 Table 2: Summary of maximum error and root mean square error (RMSE) calculated from  
941 modeled and inverted thermal diffusivities using unfiltered and filtered temperature data for the  
942 same magnitude velocity transients (0 to -1 m/d) but for different rates of velocity change. The  
943 values in this table represent a quantification of the results in Figure 8b, 8d, 8f, 8h and Figure 5b.



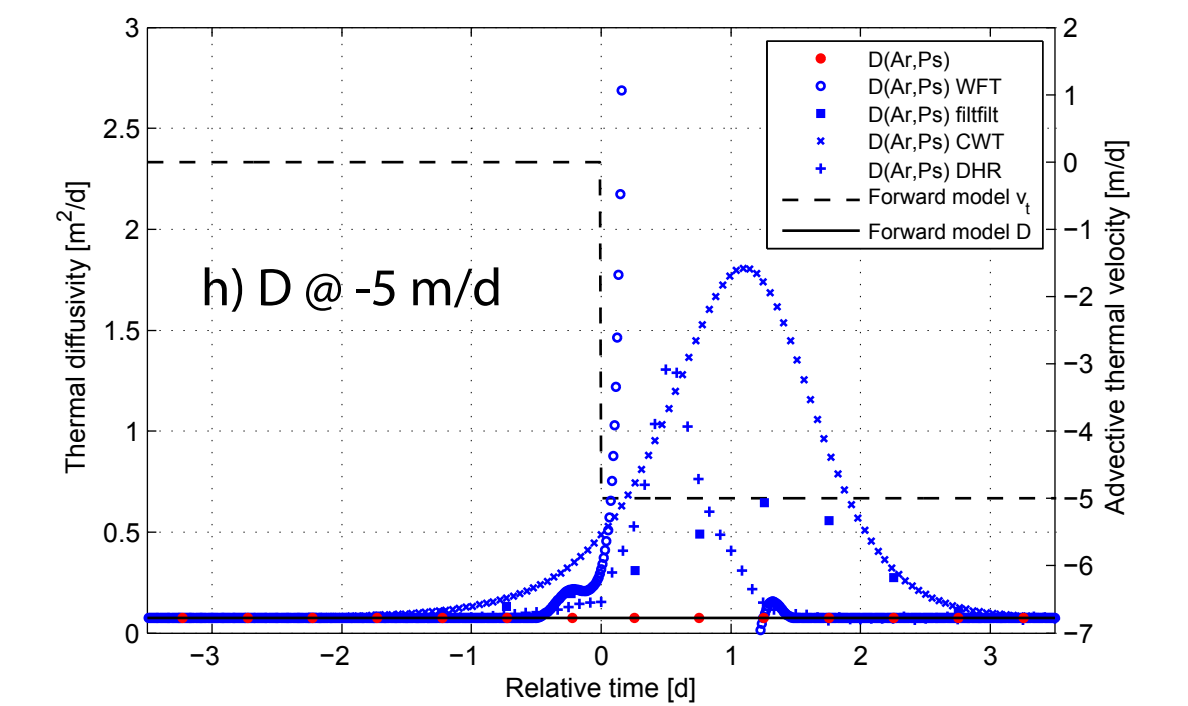
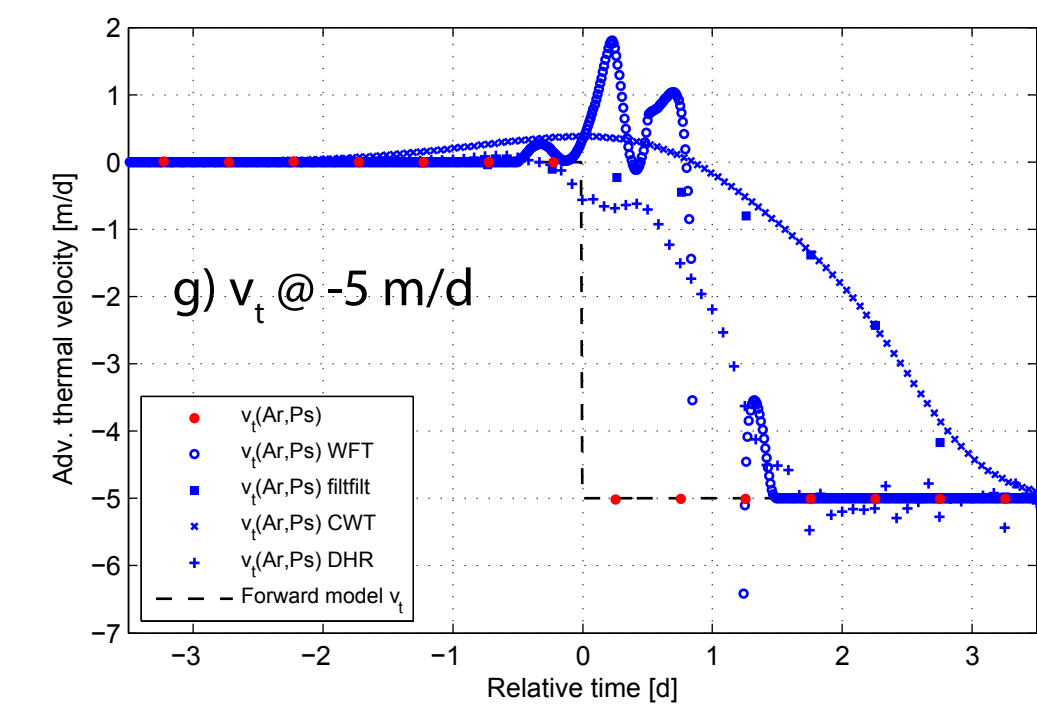
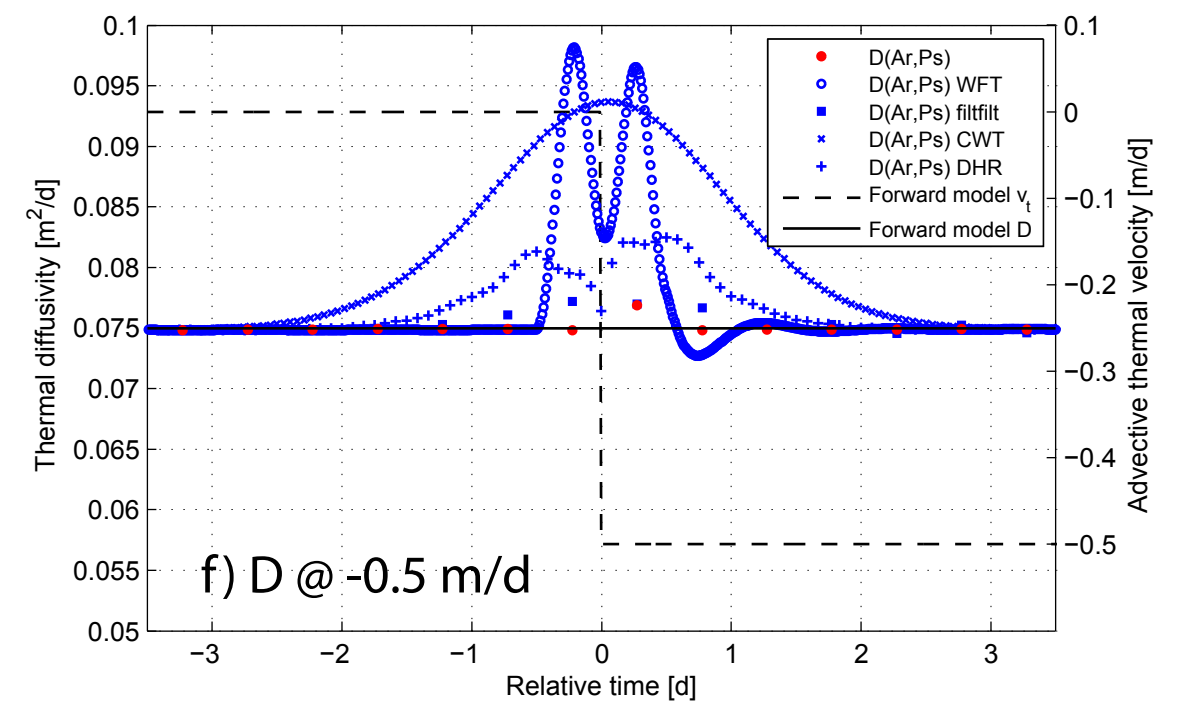
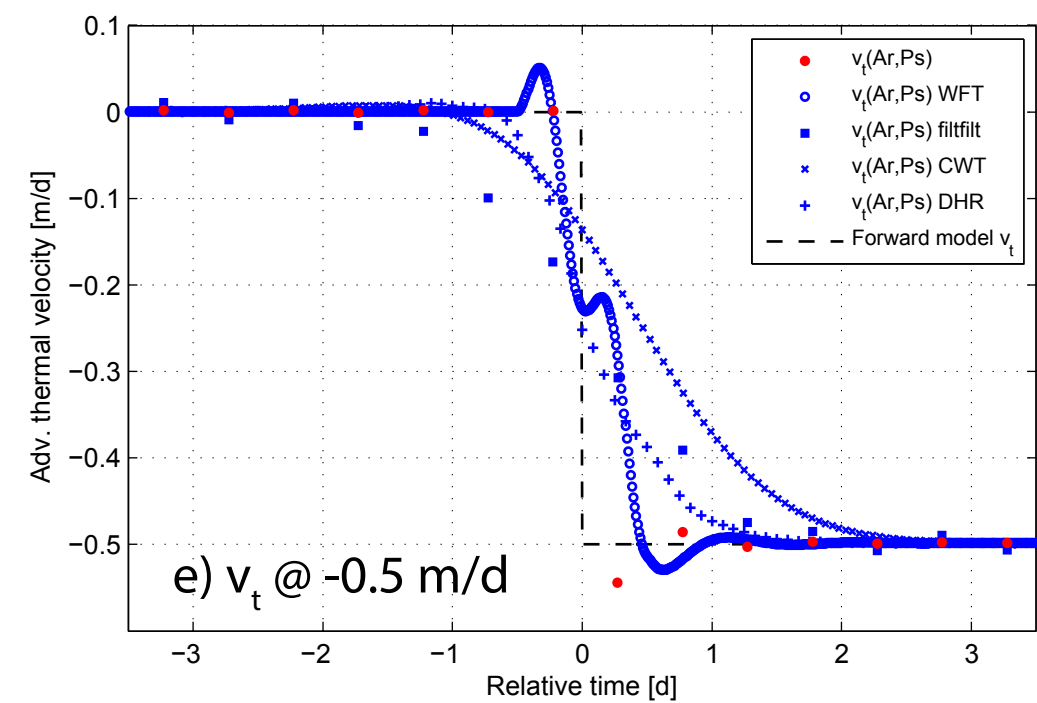
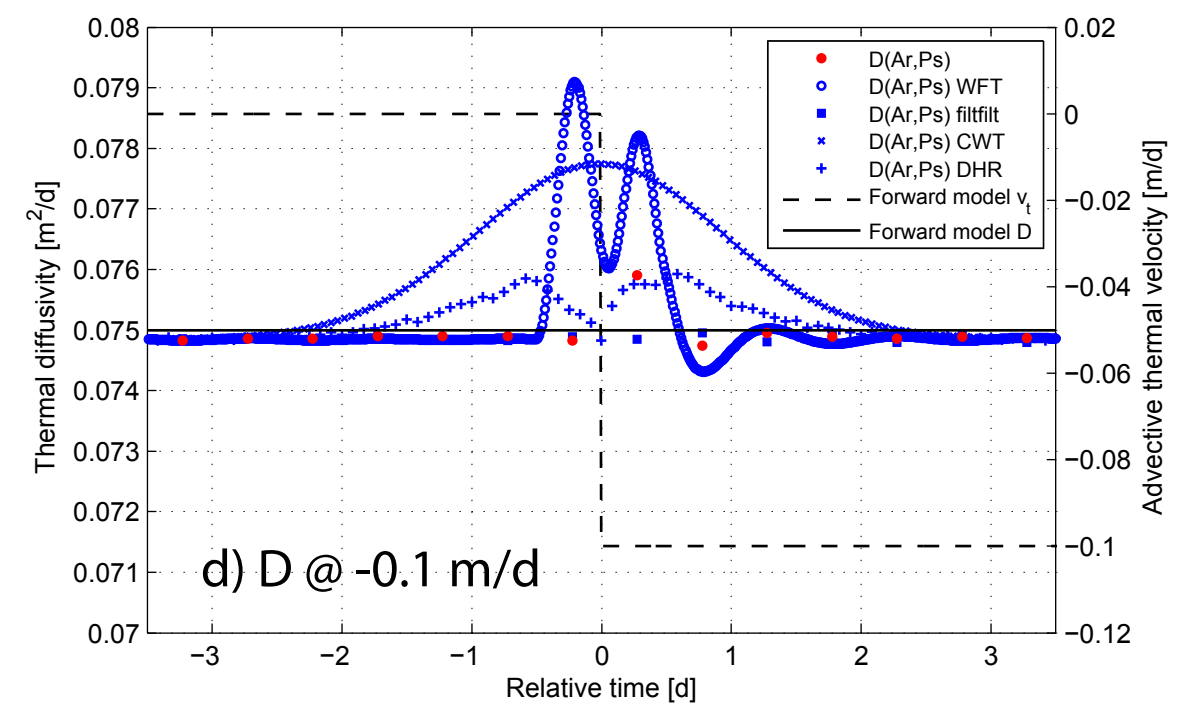
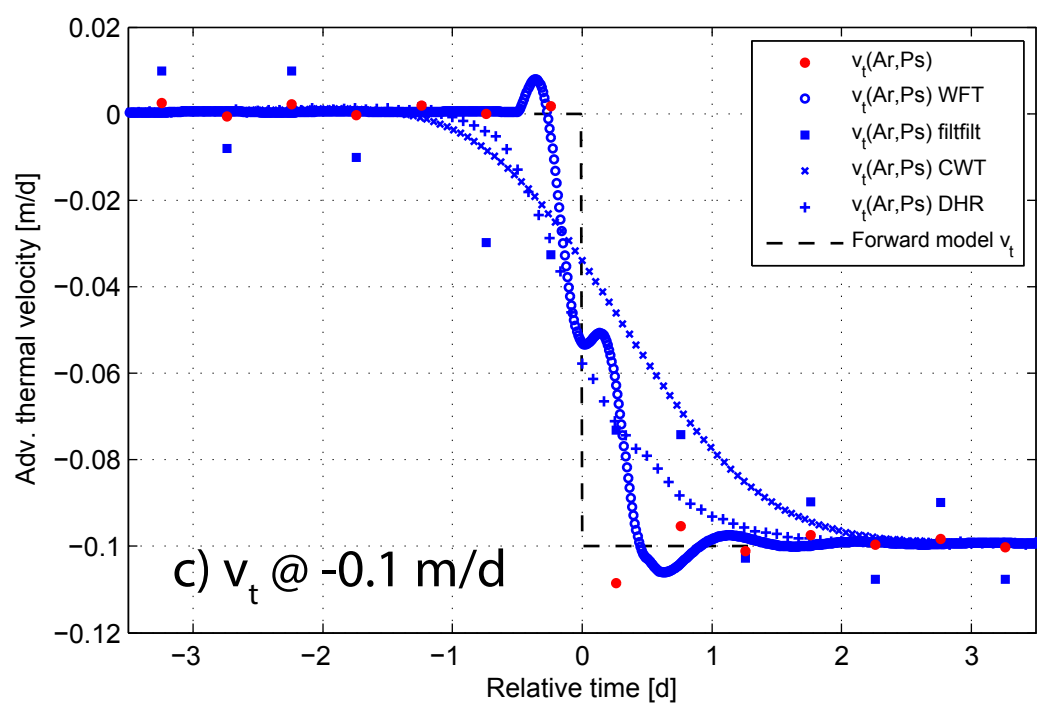
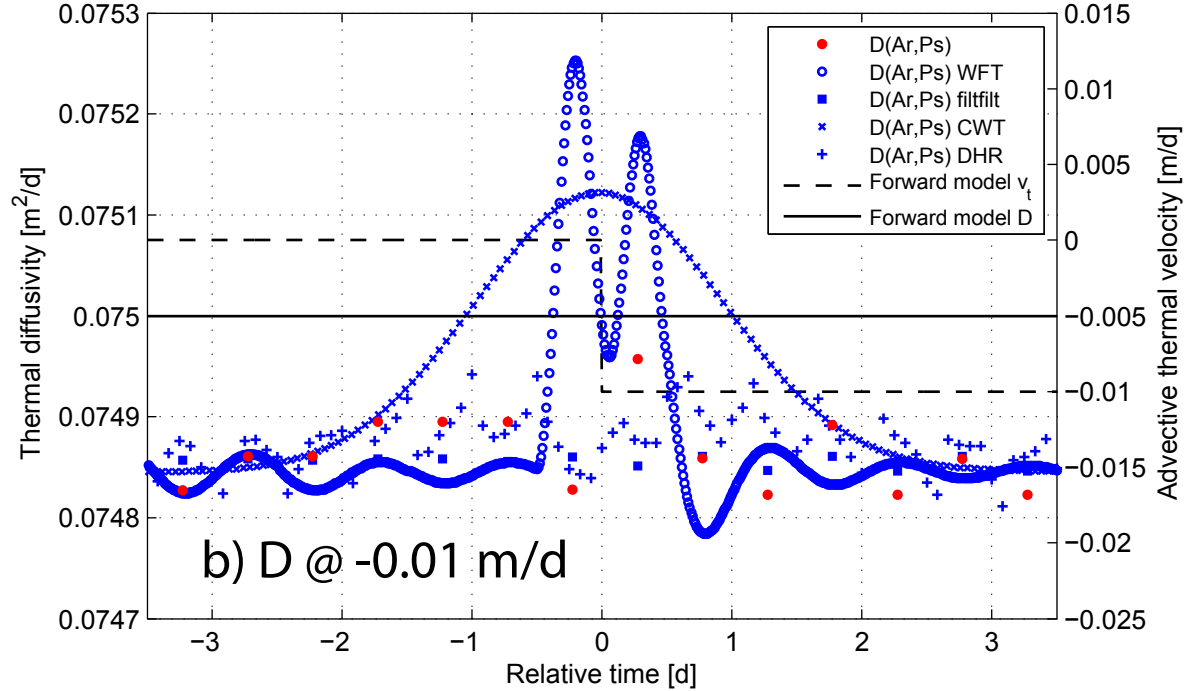
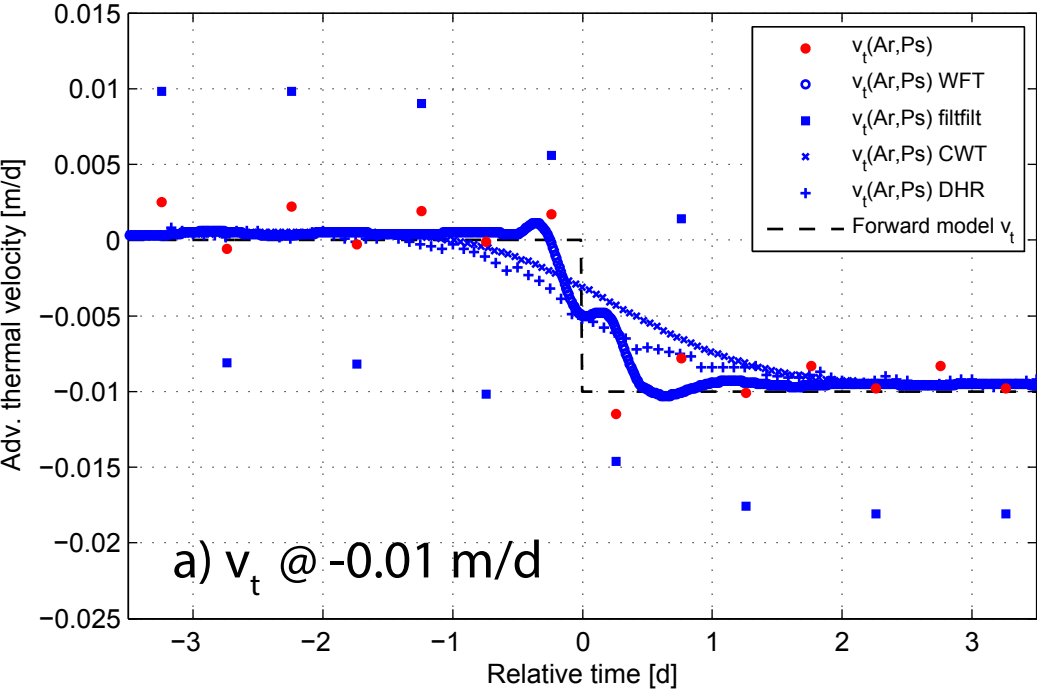


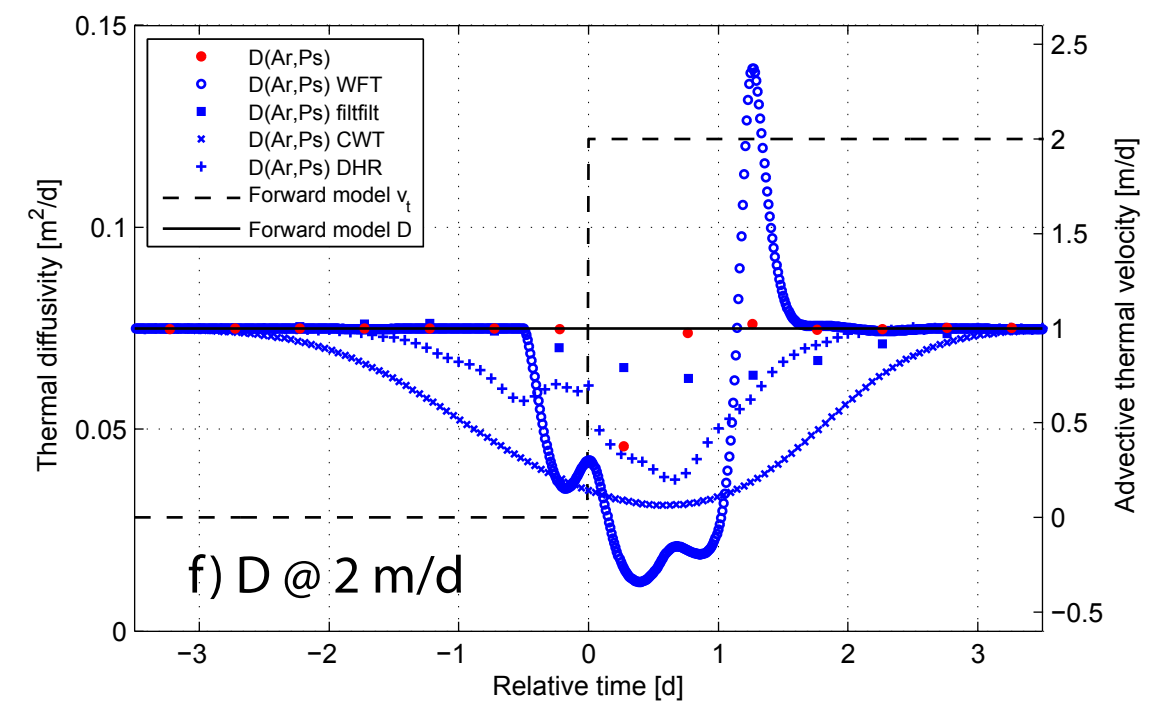
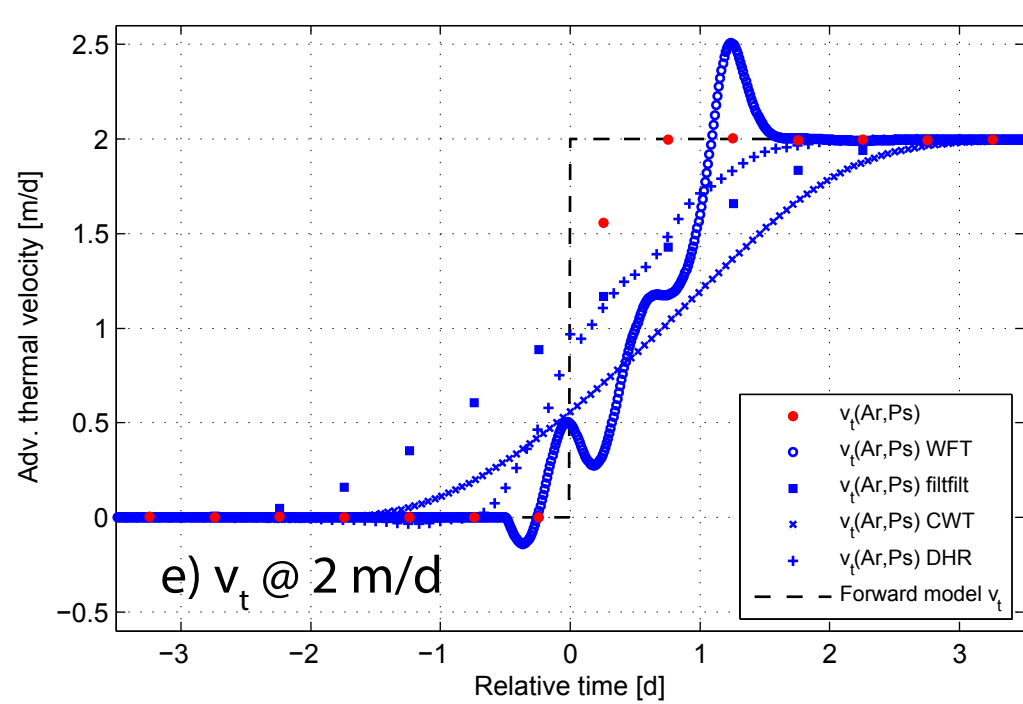
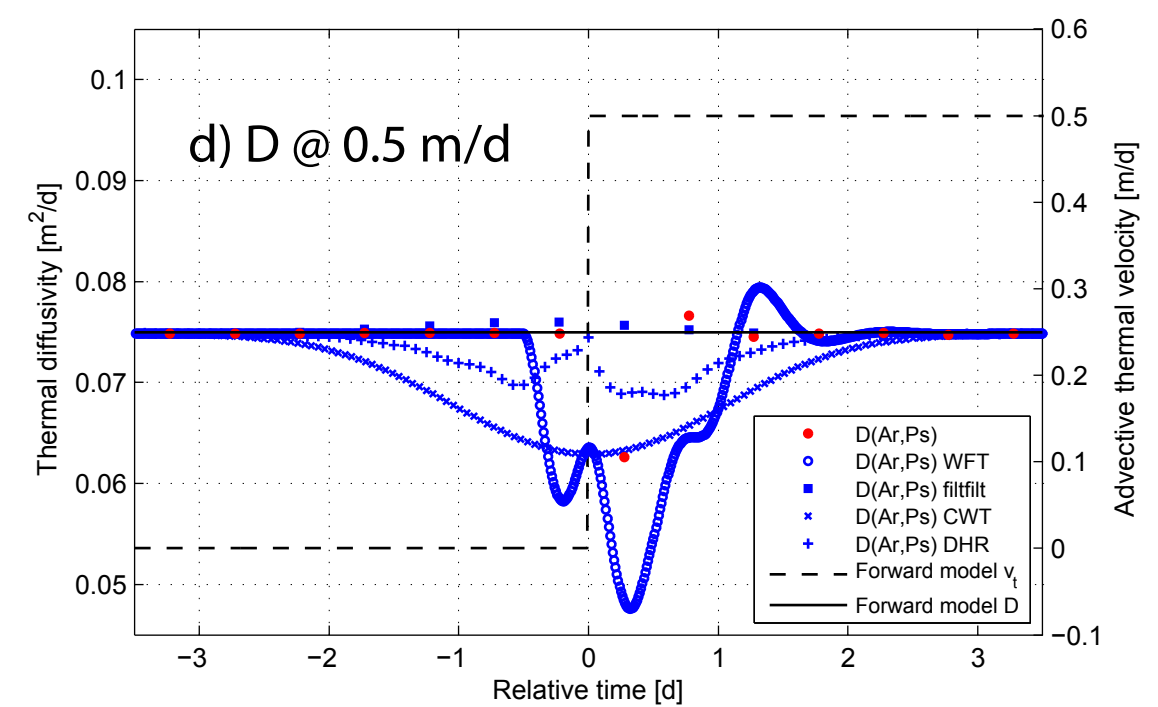
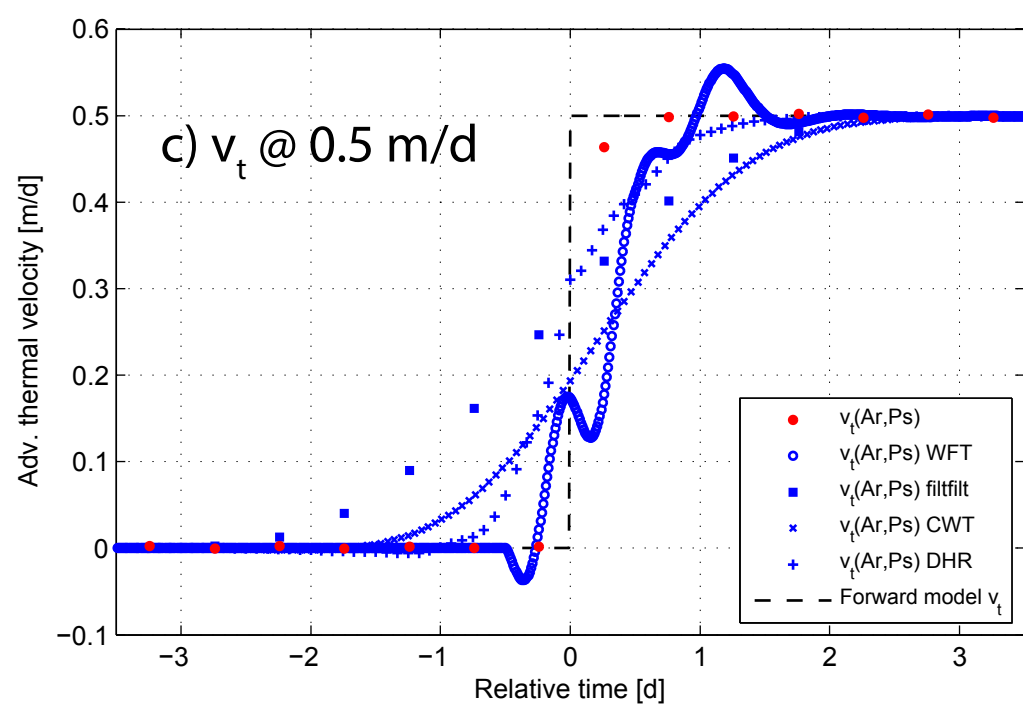
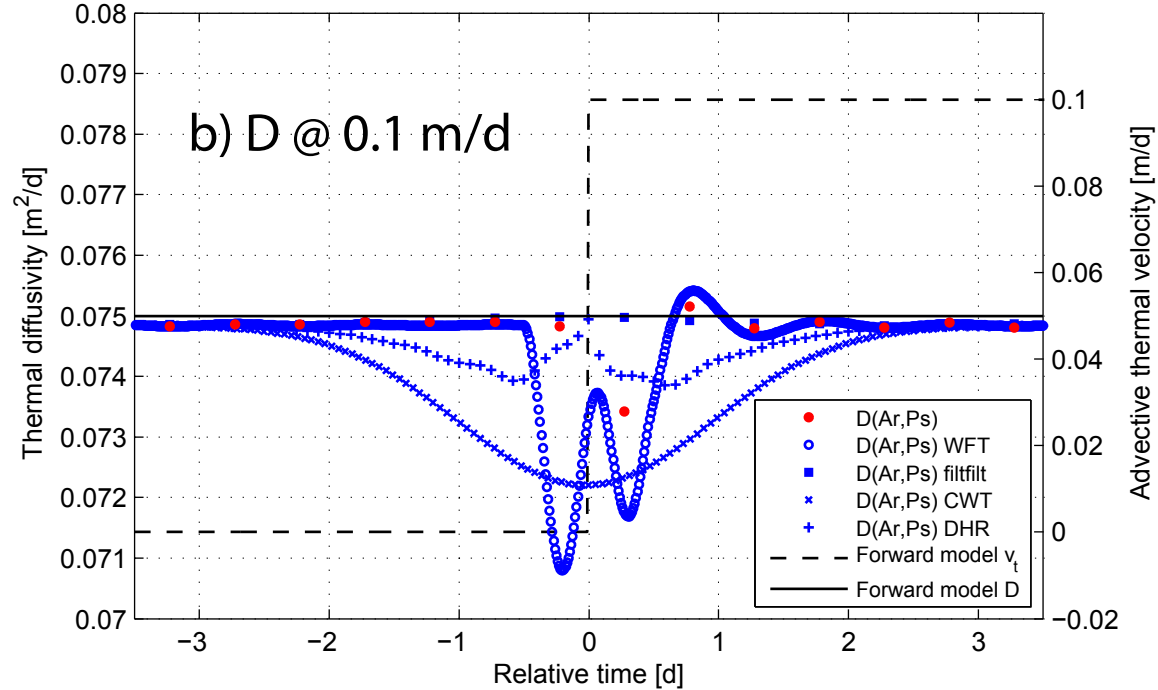
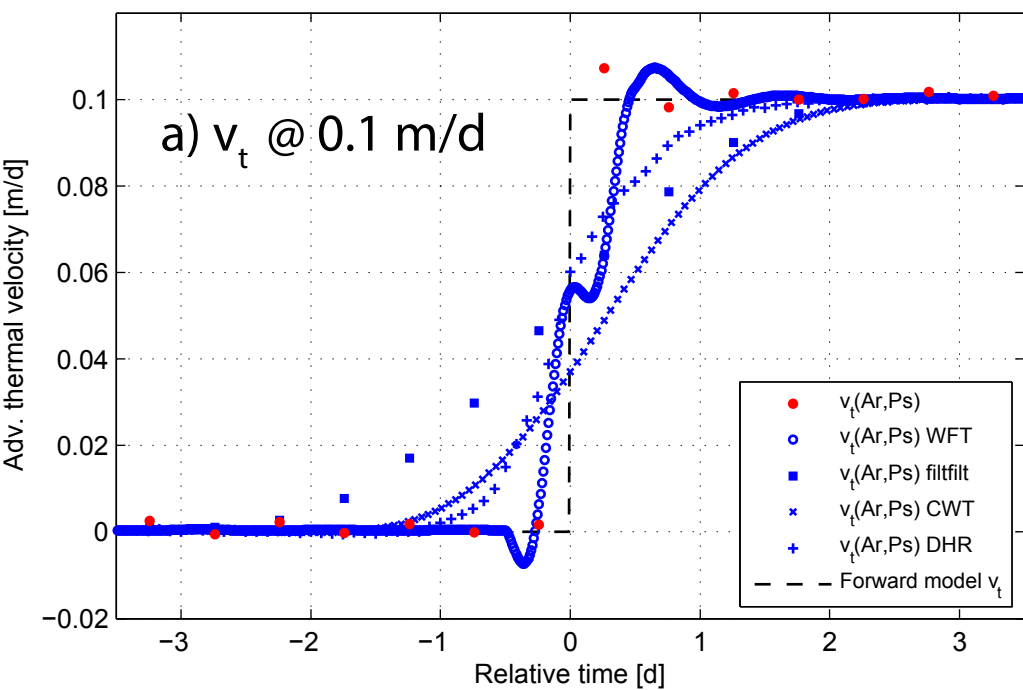


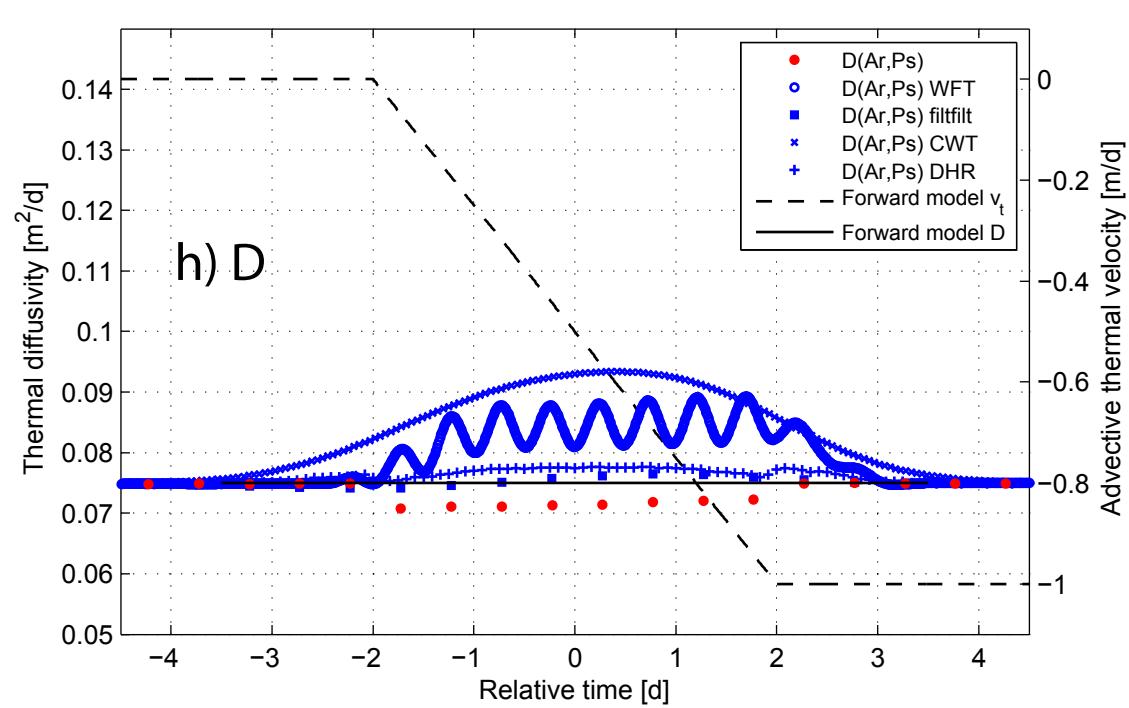
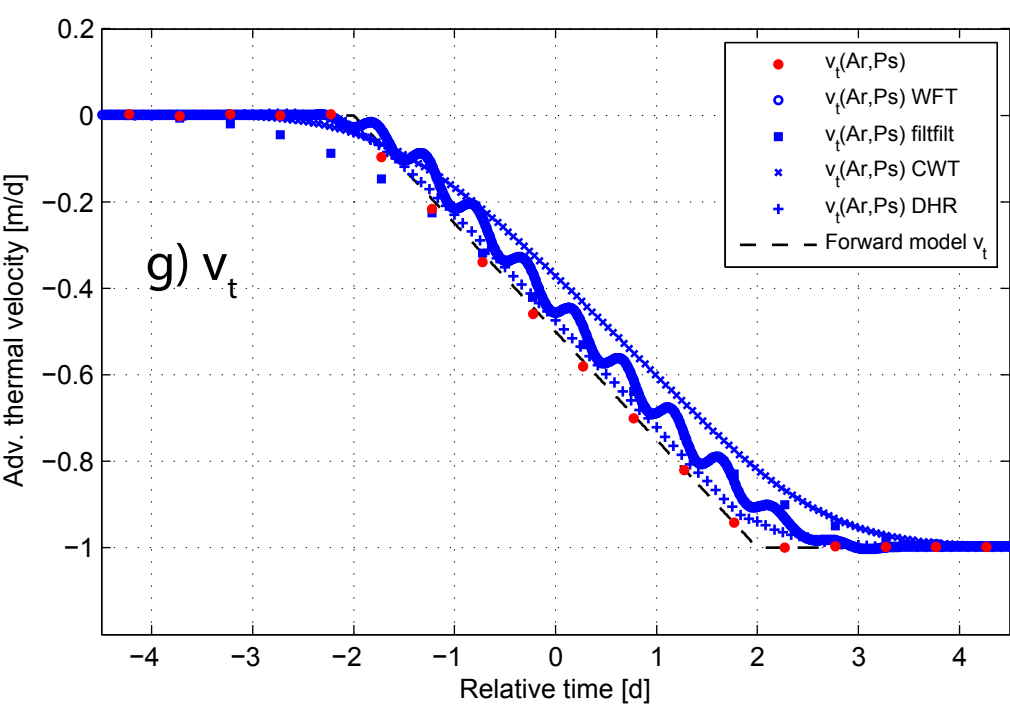
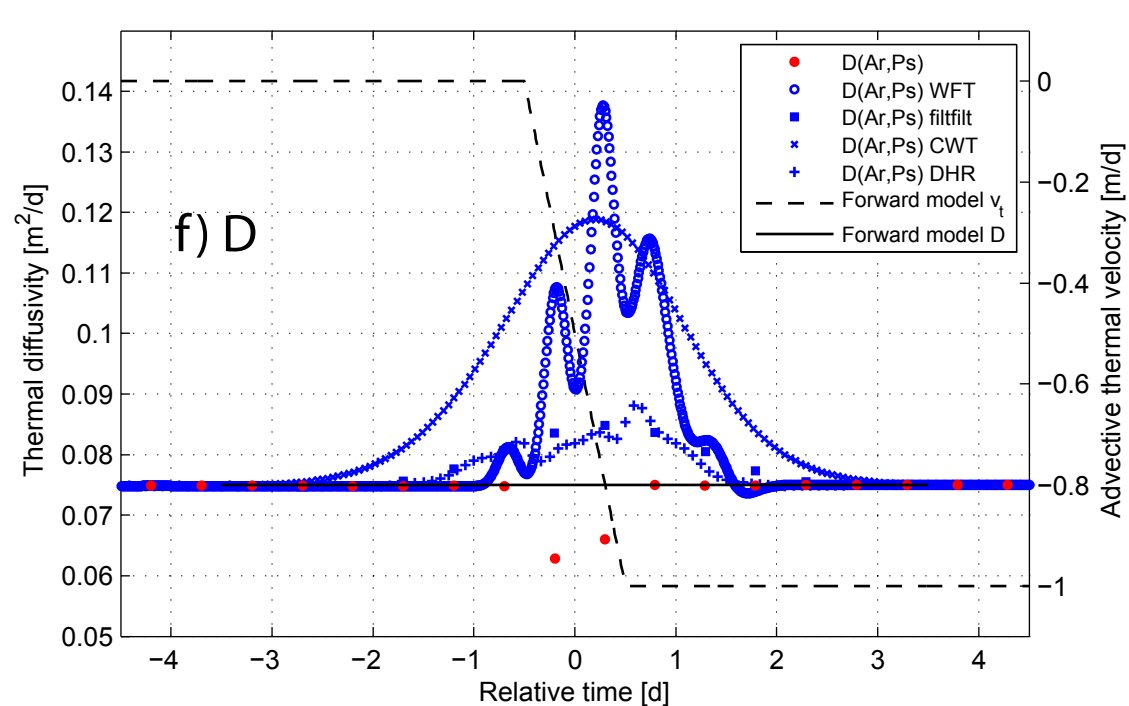
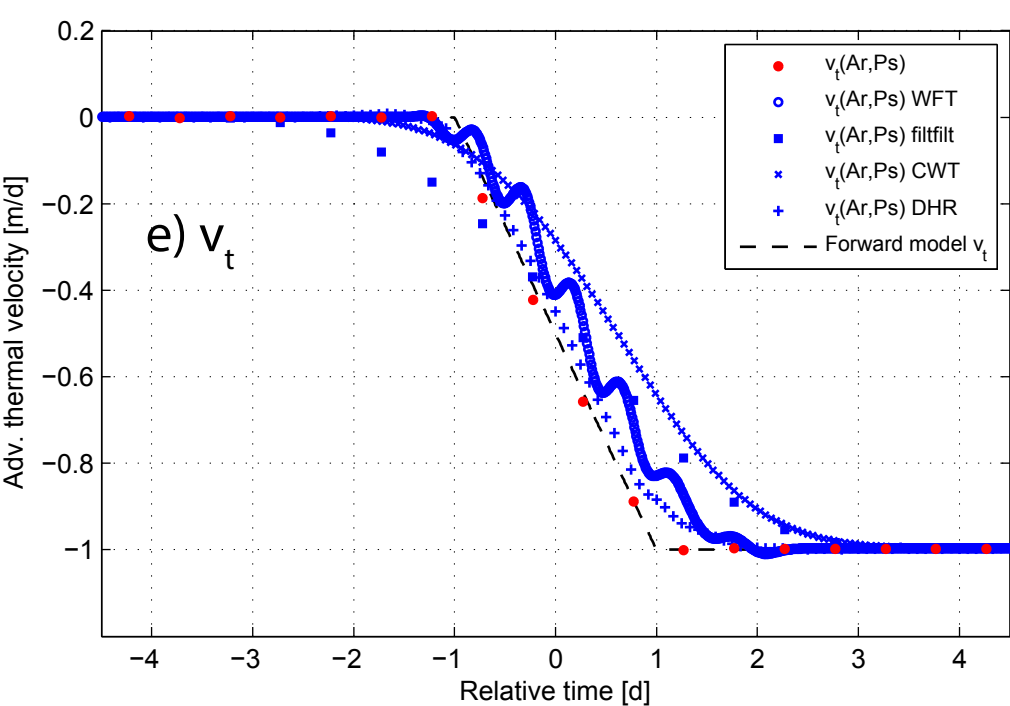
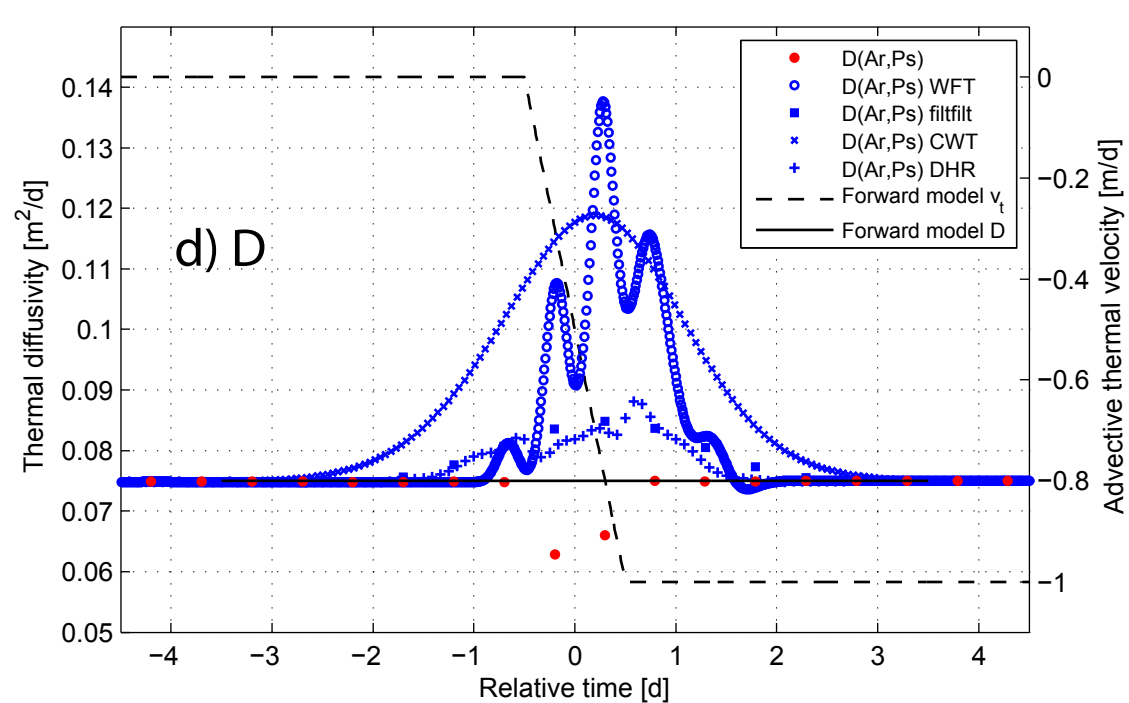
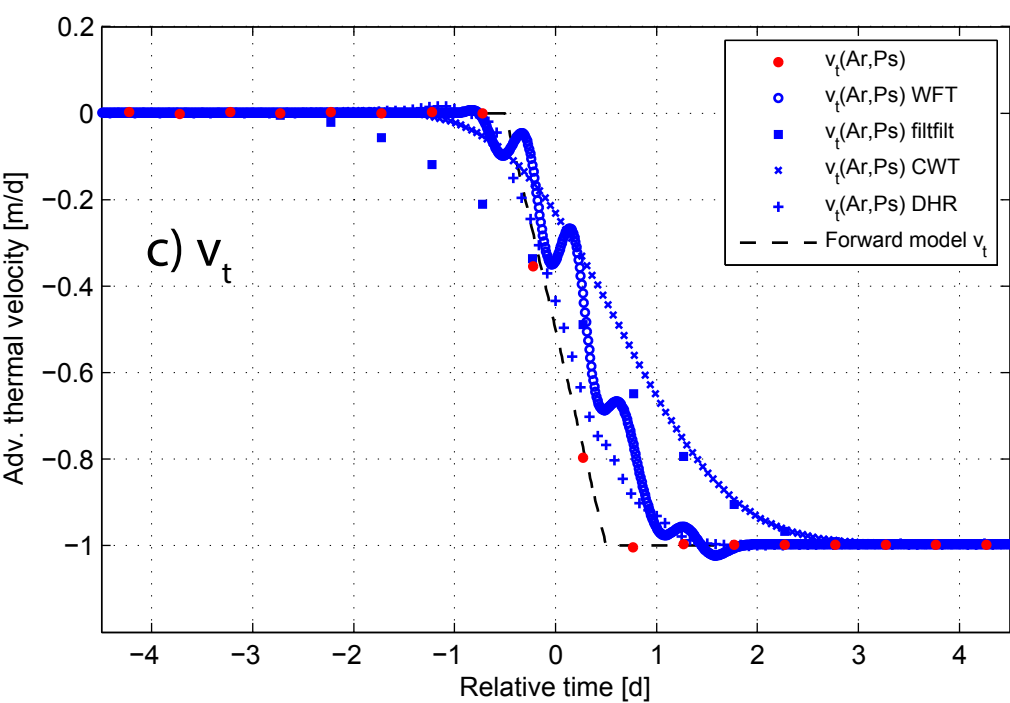
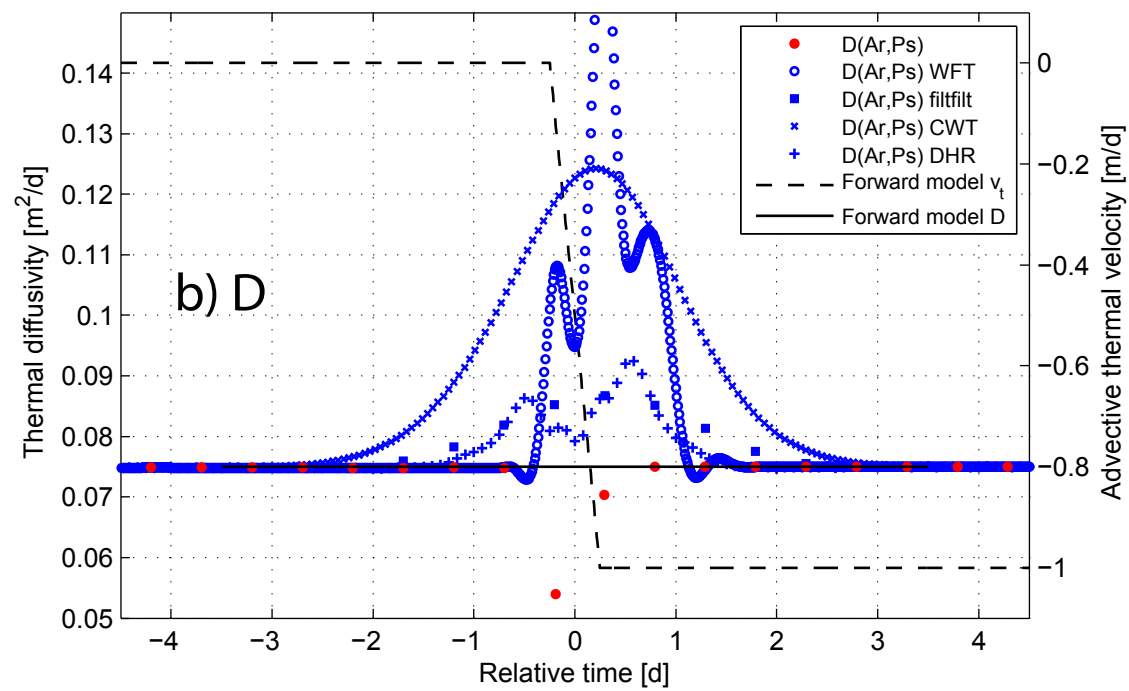
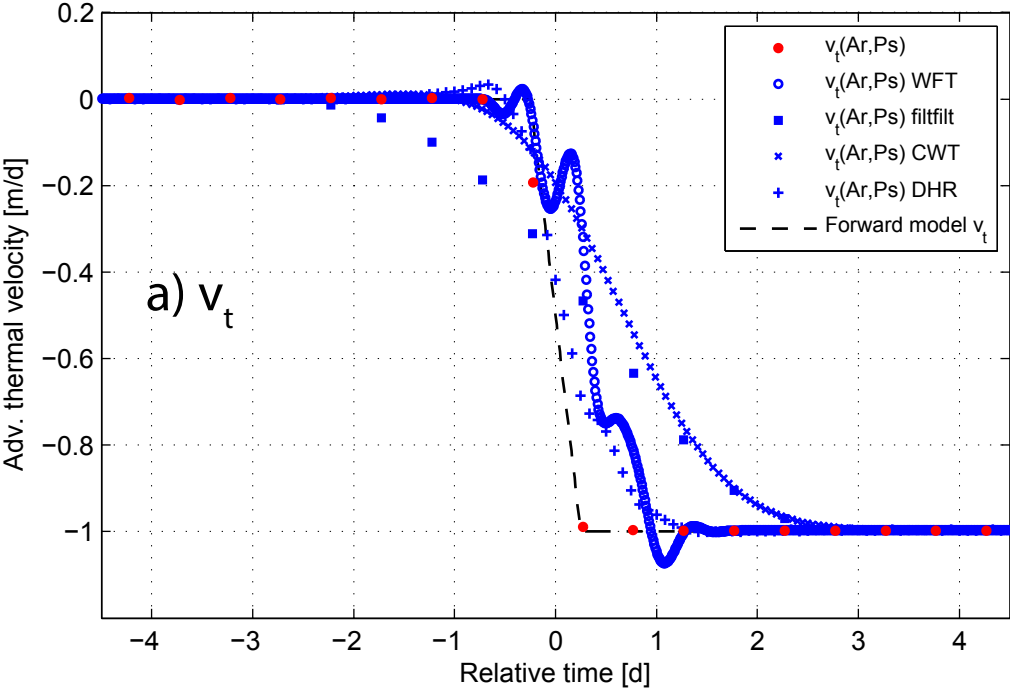


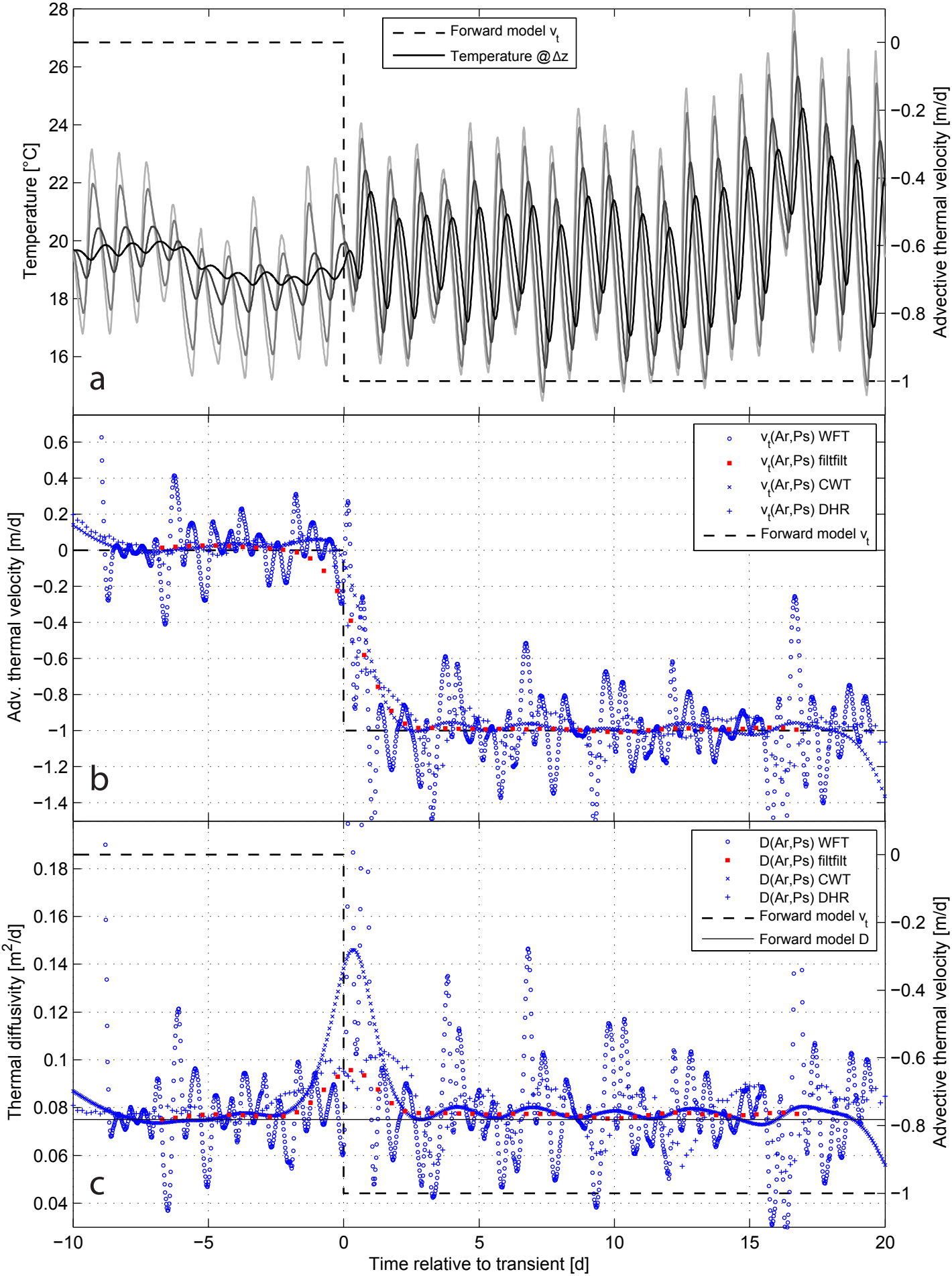












Rate of velocity change $dv/dt$ [ $L/T^2$ ]	Max. thermal velocity error [m/d]					RMSE [ $^{\circ}C$ ]				
	No filter	WFT	filtfilt	CWT	DHR	No filter	WFT	filtfilt	CWT	DHR
-0.25	-0.03	0.12	0.11	0.18	0.06	0.011	0.050	0.055	0.090	0.020
-0.5	-0.05	0.21	0.23	0.36	0.12	0.015	0.069	0.098	0.130	0.030
-1	-0.08	0.40	0.35	0.56	0.23	0.019	0.098	0.134	0.167	0.049
-2	-0.13	0.75	0.53	0.70	0.31	0.031	0.134	0.181	0.193	0.067
$-\infty$	-0.04	0.99	0.50	0.83	0.57	0.011	0.208	0.177	0.247	0.134

1

- 2 Table 1: Summary of maximum error and root mean square error (RMSE) calculated from modeled and inverted advective thermal velocities  
3 using unfiltered and filtered temperature data for the same magnitude velocity transients (0 to -1 m/d) but for different rates of velocity change.  
4 The values in this table represent a quantification of the results in Figure 8a, 8c, 8e, 8g and Figure 5a.

Rate of velocity change $dv/dt$ [ $L/T^2$ ]	Max. thermal diffusivity error [ $m^2/d$ ]					RMSE [ $^{\circ}C$ ]				
	No filter	WFT	filtfilt	CWT	DHR	No filter	WFT	filtfilt	CWT	DHR
-0.25	-0.004	0.014	0.001	0.018	0.003	0.002	0.006	0.001	0.011	0.002
-0.5	-0.008	0.030	0.005	0.032	0.006	0.003	0.010	0.002	0.014	0.002
-1	-0.012	0.063	0.010	0.044	0.013	0.004	0.014	0.004	0.018	0.004
-2	-0.021	0.097	0.012	0.049	0.017	0.005	0.018	0.005	0.020	0.005
$-\infty$	0.000	0.156	0.014	0.056	0.025	0.000	0.031	0.006	0.026	0.008

1

2 Table 2: Summary of maximum error and root mean square error (RMSE) calculated from modeled and inverted thermal diffusivities using  
3 unfiltered and filtered temperature data for the same magnitude velocity transients (0 to -1 m/d) but for different rates of velocity change. The  
4 values in this table represent a quantification of the results in Figure 8b, 8d, 8f, 8h and Figure 5b.